Experimental and theoretical investigation of mechanical responses of bacteria under hypoosmotic pressure

by

Marjan Darabi

A thesis submitted in partial fulfillment of the requirements for the degree of

Master of Science

Department of Mechanical Engineering

University of Alberta

Abstract

Bacteria represent a type of ubiquitous pathogen that respond to environmental changes such as osmotic pressure due to their cellular structure. Both Gram-negative and Gram-positive bacteria have distinct structure, including a plasma membrane and cell wall. The primary difference between them can be characterized by the absence of an outer membrane and the presence of thicker peptidoglycan in Gram-positive bacteria. While both bacterial types may exhibit different osmotic responses, the osmotic pressure-dependent mechanical responses of Gram-positive bacteria have not been thoroughly investigated, compared with those of Gram-negative bacteria. Studying the osmotic pressure-dependent morphological change and its mathematical model exert some promising utilities in biomedical applications such as designing and optimizing therapeutic strategies for drug delivery. For example, changes in cell morphology due to osmotic pressure can affect the uptake and release of drugs. Besides, mathematical models can predict how different osmotic conditions influence drug transport across cell membranes. As most of the antibiotics avoid peptidoglycan synthesis in bacteria which leads to osmotic lysis, studying structural change of bacteria under osmotic condition assist antibiotics development.

In this work, we employed a combination of experimental and theoretical approaches to study how Peptidoglycan and inner membrane deform under hypoosmotic pressure. Dynamic light scattering (DLS) analysis was used to monitor time-dependent changes in the

size of the bacteria, *Escherichia coli* (*E. coli*, Gram-negative) and *Lactobacillus acidophilus* (*L. acidophilus*, Gram-positive), over the course of incubation at different osmotic pressure conditions. Upon exposure to 300 mOsm of hypoosmotic gradient, the hydrodynamic radius of *L. acidophilus* cells was observed to increase from 0.81±0.05 μm to 1.79±0.06 μm. On the other hand, the radius of *E. coli* was found to increase from 0.45±0.008 μm to 0.67±0.01 μm at 0 mOsm. Besides, Transmission Electron Microscopy (TEM) is employed to capture morphological changes of bacteria through applying hypoosmotic pressure. The experimental results were used to develop a mathematical model. Through this model, the mechanical behavior of bacteria cell envelope is predicted by formulating equilibrium equations which describe deformations of the membrane attached to the meshed structure of peptidoglycan. This results in nonlinear partial differential equations which are solved using the custom-built Finite Element (FE) scheme. Finite Element Method, a prominent continuum approach, intricately dissects complex problems into a finite set of interconnected elements. These elements are considered continuous and deformable entities, facilitating a comprehensive analysis of the material's behavior through the examination of these discrete components.

We used Finite Element Method to elucidate the correlation between applied pressure and bacteria deformation. The numerical solver used for solving the governing equations was the Newton-Raphson method, seamlessly integrated into the FENICS platform—a Python-based open-source software dedicated to solving partial differential equations. Based on our model, it is predicted that Gram-positive bacteria experience significant out of plane deformation on z direction by increasing lateral pressure from 5 MPa to 125.30 MPa. This deformation is depicted by the red regions on the deformation contours of the model, and vividly shows that the bacteria is stretched under various pressure conditions. Furthermore, the heightened tension experienced by the bacteria in different pressure conditions is presented on Material displacement contour. It provides valuable insights into the susceptibility

of specific regions within Gram-positive bacteria to rupture under increased pressure conditions. Particularly, areas with concentrated stress and heightened strain exhibit vulnerability to rupture when exposed to elevated pressures. Notably, the maximum displacement is observed in regions of the cell where mobility along the vertical z-axis is prominent. Despite the need for further research, it was shown that theoretical predictions were well aligned with experimental findings, emphasizing the observed shape change of bacteria matching the predicted deformation.

*"In remembrance of the significant talent and cherished spirits of **Iranian students** at the **University of Alberta**, whose lives were tragically lost in the Ukrainian **PS752 flight**, this thesis is dedicated to their lasting legacy and the profound impact they continue to have on our hearts and minds"*

Acknowledgements

I extend my heartfelt gratitude to all those who have played pivotal roles in the realization and completion of this academic endeavor.

I wish to express my deep appreciation to Professor Chun Il Kim, and Professor Hyo-Jick Choi as their understanding, assistance, and support were indispensable for the successful completion of this work. Their extensive knowledge and rich experience have consistently enriched both my academic research and daily life. I would like to thank all the members of the SEED lab group, Sumin, Surjith, and Euna, and also my other teammates, Wenhao and Tahmid for their wonderful support during this journey. I express boundless gratitude to my mother, whose unwavering love and confidence have been the driving force inspiring me to pursue my study.

Contents

List of Tables

List of Figures

Chapter 1

Introduction

1.1 Microorganism Definition

Understanding higher-order evolutionary relationships among microorganisms faced challenges due to limited morphological features and a sparse microbial fossil record. Until the mid-1960s, microorganisms were primarily classified as prokaryotes or eukaryotes [1], revolutionized the field by proposing molecular sequences as documents for evolutionary history, allowing deductions based on homologous macromolecules [1], [2]. In the 1970s, Carl Woese [3], utilized molecular phylogenetics to infer evolutionary relationships among prokaryotic kingdoms, enabling universal comparisons of macromolecular features and enhancing our understanding of higher-order evolutionary relationships in microorganisms [2], [3].

Assessing microbial diversity faced hurdles, with pure culture techniques inadequately representing natural microbial communities. Standard procedures, relying on isolating strains, often overlooked predominant microbes. The challenge persisted due to the lack of suitable methods and the absence of well-developed growth conditions for many microbial species [2].

Advancements in the early 1980s, particularly in molecular phylogenetics, transformed

microbial diversity analysis. The cultivation-independent approach introduced by Stahl [4], and Pace [5], involved recovering gene sequences from microbial biomass. Small subunit rRNA genes became common phylogenetic markers due to their ubiquity. This method enabled the identification of individual population constituents, offering a more accurate and comprehensive understanding of natural microbial diversity [2]. Therefore, microorganism classification faces challenges rooted in both historical limitations and contemporary methodological constraints.

Microorganism typing involves the categorization of individual organisms based on specific criteria or analytical methods, with the choice of methods depending on the distribution and latent variation of cellular components such as sugars, lipids, nucleic acids, and proteins. While there is now a consensus in microbiology accepting phylogeny as the basis of microbial taxonomy and recognizing genome sequences as the ultimate reference for determining phylogeny, microbial systematics has traditionally been derived from comparative analyses of selected biomarkers [6]. Microorganisms such as bacteria encounter a variety of environments in their life span. Changes in pH, temperature, and concentration of external and internal solutes create conditions that might threaten the viability of bacteria [7], [8]. Especially, osmotic pressure arises as a result of the changes in internal and external solute concentration in bacteria. Increase or decrease in external osmolyte concentration provide hyperosmotic and hypoosmotic pressure across bacterial cell wall, respectively [9].

The comprehension of osmotic gradients holds paramount significance in diverse physiological processes, contributing indispensably to cellular regulation and adaptation to environmental dynamics. Within living organisms, exemplified by plants, exposure to a hypoosmotic milieu induces the absorption of water, provoking the distension of the central vacuole and instigating turgor pressure. This mechanical pressure is pivotal in averting wilting phenomena in plant tissues [10].

Marine organisms grapple with frequent hypoosmotic challenges in their habitats, a consequence of the elevated salinity inherent to seawater. These organisms regulate internal osmolarity as a strategic measure to forestall undue water loss [9]. Furthermore, hypoosmotic conditions orchestrate a facilitated uptake of nutrients within bacterial cells by fostering the flux of water and solutes. This phenomenon assumes particular relevance in nutrient-rich mediums where bacteria necessitate efficient nutrient assimilation. Additionally, hypoosmotic environments contributes to the induction of osmoregulatory protein synthesis, a pivotal cellular response to the challenges posed by altered osmotic conditions [9], [10].

Depending on the direction of osmotic gradient, water influx or outflux can be induced, resulting in change of bacterial morphology. For example, upon the generation of hypoosmotic pressure, water molecules can rapidly permeate into the bacterial cytoplasm to reduce intracellular osmolarity, creating tension in the bacteria cell wall, leading to the swelling of the cell [9]. This means that osmotic pressure-induced morphological change of bacteria strongly depends on the type of bacteria (see Figure 1.1a for Gram-negative and Figure 1.1b for Gram-positive); therefore, mechanical behavior of bacteria would depend on the wall structure [7].

1.2 Bacterial types and their structural features

Bacteria are mostly categorized into two broad groups of Gram-negative and Gram-positive, and primarily comprise the inner membrane, outer membrane, and cell wall, which are combined with various proteins [11], [12]. This classification mainly considers existing a component called an outer membrane and the difference in thickness of cell wall in both groups [7]. Gram-negative group possesses a plasma membrane and a thin peptidoglycan layer which is covered by an outer membrane, while Gram-positive group has a plasma

membrane and a significantly thick peptidoglycan layer [11], [12].

In both bacteria groups, membranes are lipid bilayers that usually contain common groups of phospholipids including Phosphatidylethanolamine as the main contributor which forms about 70 – 80% of total lipids, and phosphatidylglycerol and cardiolipin [7]. The inner membrane is placed between the cytoplasm and aqueous periplasm area and mainly consists of lipid bilayers and inner membrane proteins. The notable structural difference in bacteria types arises from an asymmetrical outer membrane as an additional layer in Gram-negative type. This membrane is made of phospholipids in the inner leaflet and lipopolysaccharide (LPS) in the outer leaflet [13]. LPS possess three different parts including hydrophobic lipid, oligosaccharide core, and a kind of polysaccharide (named O antigen) that magnify the role of the outer membrane because they form a significant portion of the outer membrane and greatly contribute to the integrity of cell structure [12], [13].

In addition to these components, different classes of protein including outer membrane proteins (OMPs) and lipoproteins (LPPs) are embedded in the outermost layer of Gram-negative bacteria [13]. The main group of OMPs is defined as Porins which are accumulated

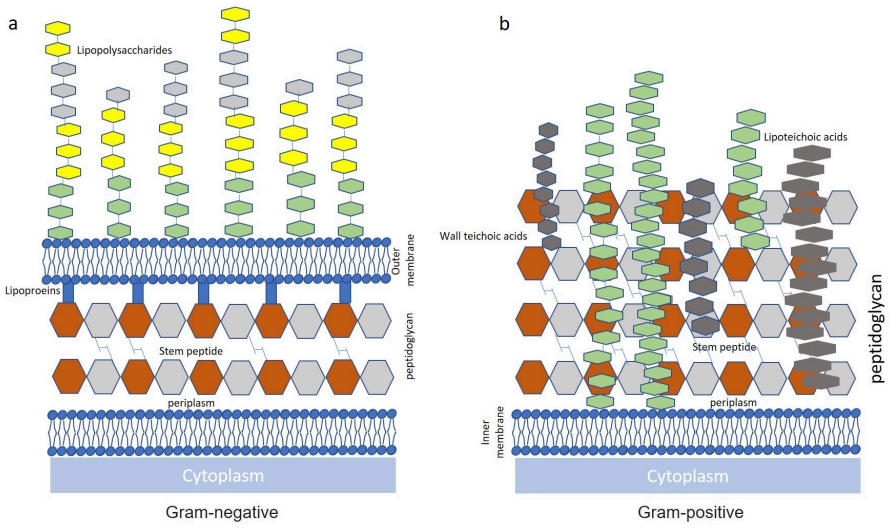

Figure 1.1: The structure of (a) Gram-negative and (b) Gram-positive bacteria.

instead of single groups and also act as channels to permeate solute molecules [13]. According to some scientific work, OMPs contribute up to 70 of the cell surface which is reported almost 500,000 in each *E. coli* cell as the most common Gram-negative bacteria type [12], [13].

Another important difference lies in the peptidoglycan cell wall, which is single-layered in Gram-negative and multi-layered in Gram-positive pathogens (Figure 1.1). The existence of glycan strands (long disaccharide chains) and peptides, which are cross-linked to each other, creates a net-like structure of peptidoglycan outside the inner membrane. These glycan strands are connected through glycosidic bonds between the carboxyl end of one glycan strand and the amino acid group in the other glycan strand [14].

From the structural viewpoint, glycan strands consist of N-acetylmuramic acid (MurNAc) and N-acetylglucosamine (GlcNAc), connecting by $\beta-1,4$ glycosidic bonds [14], [15]. Length and chain arrangement of the glycan strands play a critical role in the mechanical properties of bacteria cells [7].

In Gram-negative group, a peptidoglycan network is placed in the aqueous area of periplasm between inner and outer membranes [9]. The thickness of the peptidoglycan layer in this bacteria type is reported to be about 2.5 nm which is located in a 15 nm thick periplasm [16]. Based on some other papers, peptidoglycan thickness for single-layered Gram-negative bacteria can be increased to a maximum of three layers of 6.5 nm, while the quantity of the thickness for a Gram-positive type is extended to 19–33 nm. These numbers are obtained for the fully hydrated bacteria type [11], [17]–[20]. The cell wall is considered as the main stress-bearing element when the bacteria cell is under osmotic pressure [16].

Cell wall architecture in Gram-positive type follows either a layered or scaffold structure. In the layered arrangement, both glycan strands and peptides are connected parallelly with respect to the inner membrane, however in the scaffold model structure, glycan strands and peptides pose vertically and horizontally to the inner membrane, respectively. An example

of a layered structure in a Gram-positive group is defined in *L. acidophilus* [21], [22]. A combination of a thick peptidoglycan and inner membrane constructs the structure of *L. acidophilus* same as other Gram-positive types [20], [23], [24]. Residues of $\beta - 1,4$ which are attached to N-acetylglucosamine and N-acetylmuramic acids form sugar components of *L. acidophilus* peptidoglycan [20], [23]. Amino acids which are cross-linked between glycan chains are the other important components of *L. acidophilus* peptidoglycan. Gram-positive peptidoglycan consists of a multi-layered network of which the thickness can reach about 50 nm and carry teichoic acids (TAs) [12].

TAs are a type of linear polymers containing phosphate groups in their chemical compounds and are classified into two types lipoteichoic acids and wall teichoic acids [20], [23]. Lipoteichoic acids are one type of TAs which embedded within the peptidoglycan and linked to the inner membrane, while wall teichoic acids are only attached to the sugar backbone of peptidoglycan through covalent bond [12].

1.3 Osmotic response of bacterial cells

To gain a fundamental insight into how microbes respond to osmotic stress at a mechanistic level, it is essential to break down the intricate scenario into various components. This includes exploring the characteristics of relevant external stimuli, understanding how these stimuli are perceived, the transformation of stimuli into cellular signals, and ultimately, the creation of beneficial functional responses within microbial cells [25], [26].

The change in osmolality involves both external and internal factors. External osmolality, the primary event, takes place in the environment. On the other hand, internal osmolality is an unavoidable outcome due to the high water permeability of membranes, leading to rapid water influx in hypoosmotic conditions and efflux in hyperosmotic conditions within

milliseconds [9], [26]. Creating a functionally relevant stimulus is crucial for cellular response. Merely altering external osmolality, represented by changes in solute concentration, is not inherently considered a relevant stimulus by the cell. The cell's effective reaction relies on the presence of a stimulus, detectable by a sensor, closely mirroring the shift in external osmolality [9], [25], [26].

The cell deems a stimulus relevant through the existence of a suitable sensor system situated in either the membrane or cytoplasm. The outcome of stimulus perception is a modification in the structure or function of the sensor protein [27], [28].

For the cell to utilize a perceived physical stimulus, it must first be transformed into a mechanistically relevant signal by the sensor. Examples of such signals include conformational or structural changes in signal-transducing components, such as protein phosphorylation. Following this, the cellular signal is transduced to an appropriate target system through signal transduction [26], [28].

Upon signal transduction, the target system undergoes a change in its functional state. This can involve alterations in enzymatic activity or affinity for binding to other cellular components, such as DNA motifs or target proteins [26]–[28]. The functional changes in the target system ultimately lead to appropriate cellular responses to the primary osmotic event. These responses may include gene expression, metabolite synthesis, protein synthesis, and the activation of an enzyme or a transport protein, or structural changes in cell wall [9], [21], [26]–[28].

The structural change in the cell wall of microorganisms such as bacteria, specifically the extension of the cell wall and membrane, is considered as the cellular response to hypoosmotic pressure [21]. In contrast to the neat arrangement in the presence of hypoosmotic pressure, it has been reported that the configuration of glycan strands and peptides within the peptidoglycan is disorderly when the cell is not subjected to hypoosmotic pressure. In

contrast, when exposed to hypoosmotic pressure and experiencing stretching, these components organize themselves in an orderly manner. The covalent bonds between glycan strands, facilitated by short peptide chains in the structure, are known to sense the tension from the hypoosmotic pressure. In response, these bonds stretch, ultimately resulting in cleavage at points where the peptidoglycan is maximally extended [21].

When bacteria experience hypoosmotic pressure, they undergo swelling, causing an increase in size that eventually leads to bacterial fission or division. In response to this expansion, the peptidoglycan layer, a crucial component of the bacterial cell wall, undergoes a dynamic process. The existing peptidoglycan layer is synthesized anew, involving the breaking of existing linkages within the layer. Simultaneously, new peptidoglycan monomers are incorporated into the growing layer. Additionally, the peptide cross-links within the peptidoglycan structure need to be resealed, contributing to the restructuring of the bacterial cell wall. This process occurs in some consecutive steps [28]–[30].

At the first step, autolysins, specialized bacterial enzymes, play a pivotal role in the initial step by breaking glycosidic bonds between peptidoglycan monomers which occurs precisely at the points where the bacterial cell wall is undergoing growth [31], [32]. Concurrently, autolysins are involved in breaking the peptide cross-bridges that link rows of sugars together within the peptidoglycan structure. This controlled enzymatic activity is crucial for the subsequent steps in peptidoglycan synthesis.

In the second step, peptidoglycan monomers are transported. Peptidoglycan monomers are synthesized within the bacterial cytosol and subsequently bind to bactoprenol. Bactoprenols function as carriers, facilitating the transportation of peptidoglycan monomers across the cytoplasmic membrane. Once transported, they interact with transglycosidases [29]–[32].

In the third step, Transglycosidase enzymes, in collaboration with bactoprenols, play a crucial role in inserting and linking new peptidoglycan monomers into the breaks within the

existing peptidoglycan structure. This step is vital for the elongation and reinforcement of the bacterial cell wall [31], [32].

In the final step, transpeptidase enzymes come into play. They are responsible for reforming the peptide cross-links between the rows and layers of peptidoglycan. This enzymatic action is instrumental in fortifying the peptidoglycan structure, providing strength to the bacterial cell wall. This intricate process allows the bacterial cell to adapt and respond to changes in osmotic pressure by modifying its structural components [28]–[32]. Peptidoglycan's role in hypoosmotic pressure response is acknowledged, but the primary detectors and responders to such pressure are the inner membrane components, particularly embedded proteins. These proteins are instrumental in relieving sensed lateral pressure, acting in parallel to the cell membrane, rather than perpendicular [33], [34].

Since the discovery of mechanosensitive channel (MS) activities in bacterial cell membranes in 1987 [35], researchers have made significant strides in understanding the physiological functions, structural models, and sensing mechanisms of these channels [36].

In the historical context of electrophysiology advancements, Ching Kung's group in Madison, Wisconsin, conducted patch-clamp experiments on native bacterial membranes [36], [37]. By generating patchable-sized cells from *E. coli* through a technique involving giant cells or spheroplasts, they observed mechanosensitive channel activity as a response to suction, a tension-inducing stimulus applied through hollow electrodes and tubing [35], [38]. Surprisingly, these channels opened in response to suction, and subsequent studies indicated their activation by amphipaths, suggesting sensitivity to changes in the lipid environment [39]. Further investigations across bacterial species revealed the common presence of mechanosensitive (MS) channels in both Gram-negative and Gram-positive organisms [36], [40], [41].

Mechanosensitive channels with nano-sized pores are triggered by tension detected within the lipid bilayer. Upon the application of hypoosmotic pressure to the cellular structure,

these MS channels undergo gating, permitting the release of osmotically active solutes and ions from inside the cell while allowing water influx. This process ensures equilibrium between internal and external solute concentrations by expelling excess solutes, preventing osmotic cell rupture. The opening and closing of MS channel proteins occur rapidly, closing promptly upon the alleviation of tension [33].

Bacteria typically feature four prevalent mechanosensitive channels governing hypoosmotic pressure: Large Mechanosensitive Channels (MscL), Small Mechanosensitive Channels (MscS), Miniconductance Mechanosensitive Channels (MscM), and Potassium-Dependent Mechanosensitive Channels (MscK) [33], [42]. Within the mechanosensitive (MS) classification, additional channels such as YbdG, YnaI, YbiO, YjeP, or KefA are subcategorized within the main groups. Nevertheless, MscL and MscS appear to hold a more prominent role compared to the other groups [42]–[44]. That is, bacterial strains possessing either MscS or MscL mechanosensitive channels can withstand hypoosmotic gradients. MscS and MscL, functioning as tension-sensing gates, exhibit distinct opening ranges at tensions between 5-8 mN/m and 9-15 mN/m, respectively [34], [42].

In other words, the bacterial mechanosensitive channels, notably MscL and MscS, are the only bacterial channels with a well-defined physiological function. Initially speculated to be involved in osmotic regulation, these channels were thought to play a role in responding to changes in osmolarity. In high-osmolarity environments, bacteria accumulate compatible solutes like proline, betaine, trehalose, and potassium to maintain high cell turgor [36], [45], [46].

A sudden decrease in osmolarity, referred to as downshock, can lead to a rapid release of these solutes, causing an increase in cytoplasmic pressure [47]. The bacterial MS channels are believed to act as emergency release valves, preventing cell lysis by facilitating the expulsion of solutes in response to extreme decreases in the osmotic environment [36]. It is interesting

to note that in earlier literature, the efflux was believed to be facilitated by multiple channels specific to different solutes [36].

Following mechanosensitive channel discovery, the MscS and MscL channels were considered potential candidates for osmotic regulation due to their activity and selectivity. Although the MscL null strain showed no obvious phenotype, suggesting redundancy with MscS, some mutagenesis studies demonstrated that changes to MscL could lead to osmotic phenotypes [48]. Marine organisms typically lack MscL, presumably due to the absence of osmotic shifts [49]. Expressing *E. coli* MscL in the marine bacterium Vibrio alginolyticus alleviated osmotic downshock cell lysis, indicating a role in osmoregulation [50].

The identification of the MscS gene and the observation of an osmotic-sensitive phenotype in an MscS MscL double null strain provided firm evidence that MscS and MscL play a crucial role in adapting to rapid decreases in the osmotic environment by facilitating the efflux of accumulated solutes [36], [51].

1.4 Mechanosensitive channel structure

Due to the significant role of mechanosensitive channels in transferring water and other solutes such as sugar, the structures of MscL and MscS channels have been extensively investigated [33], [43], [52].

The structure of mechanosensitive channels is defined by its subunit configuration [34], [42]. MscL is composed of five subunits, each possesses transmembrane α–helices of 1 and 2 (i.e., TM1 and TM2), a periplasmic loop, and N-terminus and C-terminus domains (Figure 1.2) [33], [42], [43], [52], [53]. When the channel is exposed to tension, transmembrane domains in each subunit sense the force and undergo a conformational change from closed to open (Figure 1.3) [33], [43], [52], [53].

After resolving the crystal structure, researchers speculated on the open-state structure of the MscL channel, considering the challenge posed by its large pore size. Early models suggested thinning of the channel in the membrane plane, resembling the iris of an old-fashioned camera, as opposed to the idea that all transmembrane domains contribute to the pore's expansion [36], [53]. Despite membrane limitations in tension, MscL can compress and expand within the membrane during gating, causing structural changes in lipids and altering protein-lipid interactions [54], [55]. This iris model aligned with structural studies using electron paramagnetic resonance and FRET spectroscopy supported this model [56], [57].

Scientific literature indicates that MscL exhibits a diameter extension of approximately 30–40 Å [44], [57], representing a significant conformational change. Under membrane tension, MscL undergoes flattening along the pore axis, attributed to a pronounced tilt in the TM1 and TM2 helical regions [33], [43], [52], [53].

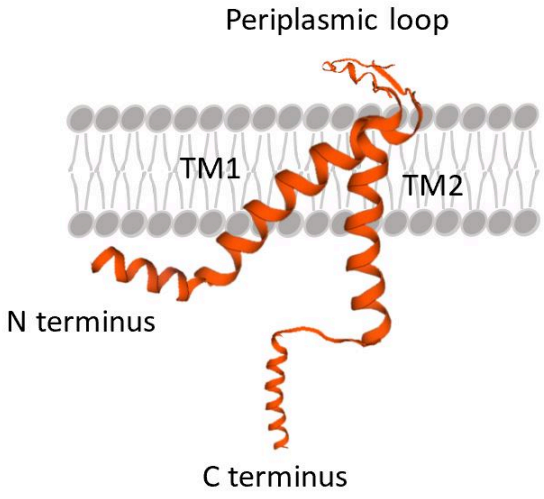

Figure 1.2: The structure of a MscL channel inside the inner membrane of Mycobacterium tuberculosis. Reprinted from [43].

The crystal structure of MscS resolved at 3.95 Å, has revolutionized our understanding of the protein [58]. MscS, a crucial channel protein, features a heptameric assembly with seven subunits arranged around a rotation axis parallel to the membrane. Each monomer consists of three N-terminal helical regions, namely TM1, TM2, and TM3, the latter being split into TM3a and TM3b (a cytoplasmic-facing helix) [59].

Each subunit's arrangement forms a cytoplasmic cage through the configuration of the middle β domain and an α–β domain (Figure 1.4) [43]. The central pore is created by TM3a helices and is capped at the top and bottom, enclosing a ring of compact α–β domain [59].

The interface between these domains creates a conduit for the passage of ions and solutes. The coordinated movement of Transmembrane 1 and 2 results in the packing of the TM3a helix, inducing an open conformation with a diameter ranging from 13 to 14 Å [43], [52], [58]. Therefore, the identification and examination of mechanosensitive channels in bacteria have triggered a profound shift in our understanding of bacterial physiology. Although, understanding MS proteins, requires acknowledging the essential partnership between the protein and the lipid bilayer [59].

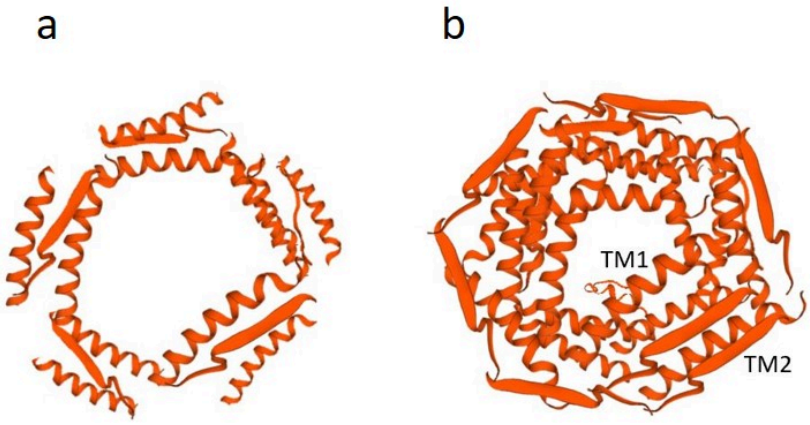

Figure 1.3: The structure of a MscL channel inside the inner membrane of *E. coli* which is viewed from above in a) open and b) closed structure. Reprinted from [43].

The lateral pressure profiles of the bilayer reveal that the junction between the head group and the lipid chain experiences the highest tension [60]. The hydrophobic region of the bilayer corresponds to approximately 32 Å [61], and when considering glycerol residues and head groups, an additional 30 Å is added [62]. The hydrophobic regions of membrane proteins are expected to align with the equivalent regions of the bilayer, with the tension-sensing regions of the channel positioned at the interface where relatively hydrophilic residues interact with the polar components of the glycerol-phosphate-ethanolamine [63].

MscS potentially interacts with lipids at three main sites: the N-terminal sequence (residues 1–27), TM1-2, and TM3b [59], [64]. While genetic evidence indicates that residues near the N-terminus influence channel gating, the exact interaction of the surface of TM3a facing the bilayer remains untested. The Trp residue at position 16 in *E. coli* MscS is crucial for pressure sensitivity, as substitutions with similar residues (Phe, Tyr, Leu) result in

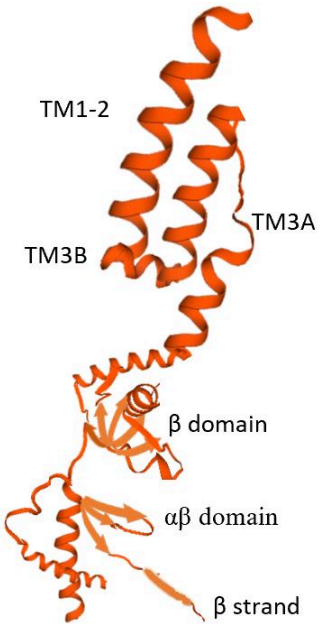

Figure 1.4: The structure of a MscS channel inside the inner membrane of *E. coli*. Reprinted from [52].

reduced pressure sensitivity, indicating a higher pressure requirement for the closed-to-open transition in mutant channels [64]. The absence of these residues in the crystal structure is a notable limitation in understanding these interactions [59].

TM3b in MscS is amphipathic, with hydrophobic residues projecting toward the bilayer in the crystal structures, suggesting that this helix may reside in the head group region. This arrangement allows the hydrophobic residues to contact the lipid chains, with the head group region being deep enough to accommodate an α–helix [62]. At the end of TM3b, conserved Arg residues (Arg128 and Arg131) can bond to the phosphate head groups of the bilayer, providing a peripheral anchor for the vestibule of MscS [59].

The primary focus for tension sensing in both MscS and MscL is the TM1-TM2 interface region situated within the lipid bilayer. Mutations that impede gating are frequently clustered near the boundary between the head groups and the lipid chains, underscoring the pivotal role of this region in tension sensing [65], [66]. Rather than the presence of specific residues, mechanosensing behavior appears to stem from the absence of such residues.

Mutations hindering gating in MscS and MscL involve the replacement of hydrophobic residues with those promoting hydrogen bonding at the TM1-TM2 interface [65]. Conversely, substitutions in other segments of the transmembrane helices, projected to reside deeper within the lipid phase, result in channels gating at lower membrane tensions [65], [66]. This emphasizes tension sensing as a consequence of reduced hydrogen-bond-favoring residues specifically at the TM1-TM2 interface. In contrast, the presence of similar mutations in other regions may influence the tension threshold at which the channel gates [59]. Non-mechanosensitive membrane proteins, enriched with residues favoring hydrogen-bond formation at the interface region, tend to stabilize in the bilayer without significant structural transitions in response to changes in membrane tension. This stands in contrast to MscS and MscL, which undergo rearrangements to form open pores under tension [59], [63].

1.5 Aquaporins

Aquaporins (AQPs) are the other important transmembrane channel proteins in the inner membrane which facilitate water permeation and, in some cases other solutes such as glycerol through the membrane. Their primary function is to facilitate the passage of water and small solutes into and out of cells and organelles [67]. In other words, they transport water to both sides of the membrane depending on the osmotic pressure, to reduce concentration gradient and help in osmoregulatory response [68], [69]. The diverse roles played by AQPs in living organisms, sometimes extending beyond conventional expectations, make them subjects of extensive research.

Primarily, AQPs are divided into two subgroups of classical aquaporins and aquaglyceroporins to permeate water and glycerol molecules, respectively [69], [70]. Classical aquaporins transfer water and AQP1 is the most investigated aquaporin which was examined through crystallography analysis [68], [69], [71].

Aquaporins (AQPs) are characterized by a homotetramer unit containing six transmembrane domains, and their NH2- and COOH-termini are located in the cytoplasm (Figure 1.5) [72]–[74]. The distinctive feature of AQPs is the presence of two conserved hydrophobic stretches of amino acid residues known as asparagine-proline-alanine (NPA) boxes, serving as the signature sequences for this family [72], [73]. As genome projects advance, the identification of AQP-like sequences is increasing based on amino acid sequence similarities, particularly in the regions surrounding NPA boxes. While some of these sequences may belong to the AQP family, many remain uncharacterized functionally. Some exhibit unique primary structures with additional residues at the NH2- and/or COOH-termini, or they may result from alternative splicing [74], [75].

Aquaporins (AQPs) exhibit a consistent three-dimensional (3D) tetrameric structure, featuring a central pore in each subunit [76], [77]. Some AQPs possess larger pores, facilitating the permeation of glycerol and potentially urea [78]. These structural analyses offer insights into the substances that can traverse the channel and the regulatory mechanisms, including phosphorylation or interactions with NH_2-terminal residues [79]. Moreover, surprising non-transport functions of AQPs have been unveiled, involving cell adhesion through the formation of junctions with the plasma membrane, interacting with opposing AQPs molecules. While this nontransporting role is increasingly acknowledged, its physiological significance remains to be further confirmed [80].

The other porins group is aquaglycerolporins which introduce a new group of aquaporins as they are permeable to glycerol as well as water [81]. These two porin channels are fairly similar with some differences in residues at the narrowest sections of the channels [81], [82]. As bacteria are one of the main microorganism groups, they also contain water and glycerol transporting channels in their inner membranes, such as AQPz and GLPF as the most studied ones [69], [81], [82].

As the structure of AQPz is determined to be similar to AQP1, they also contain six transmembrane regions and five loops (Figure 1.5). Loops B and E contain two asparagine–proline–alanine (NPA) motifs which are embedded in the inner membrane. Besides, loop C is the longest one in the structure. AQPz is considered as a highly-tight tetrameric structure [72], [81].

The structure of AQPz was investigated by Savage. et al [83], and showed great similarities with AQP1. The constriction site in this aquaporin type is narrowed to about 2 Å and is formed through Arg189, Phe43, His174, and Thr183 chains [82]. This pore provides hydrophilic N-terminal and hydrophobic C-terminal sides which the N-terminal contains four carbonyl groups of Gly59, Gly60, His61, and Phe62 and C-terminal contains four carbonyls of Asn182, Tyr183, Ser184, and Val185 [82]. Similar to the other AQPs, the central region of the membrane pore is slender, but it expands both above and below to create periplasmic and cytoplasmic passages [81].

Glycerol facilitators (GLPF) transfer glycerol not water, and is characterized in *E. coli* through X-ray crystallography [69], [81], [84]. AQP1 and GLPF showed a relatively similar structure including six α–helix transmembrane domains as well as three extracellular and two cytoplasmic loops (Figure 1.6). The difference between these two structures is the arrangement of extracellular loops. For example, GLPF possesses a significant short loop A compared to AQP1. Besides, loop C which is responsible for the connection between two tandem repeats, forms a relatively flat surface in AQP1, while GLPF has an extended loop C containing a helix-turn-helix motif. In terms of loop E in the second tandem repeat which carries the NPA motif, is more extended in GlpF than in AQP1. This loop forms a one-turn

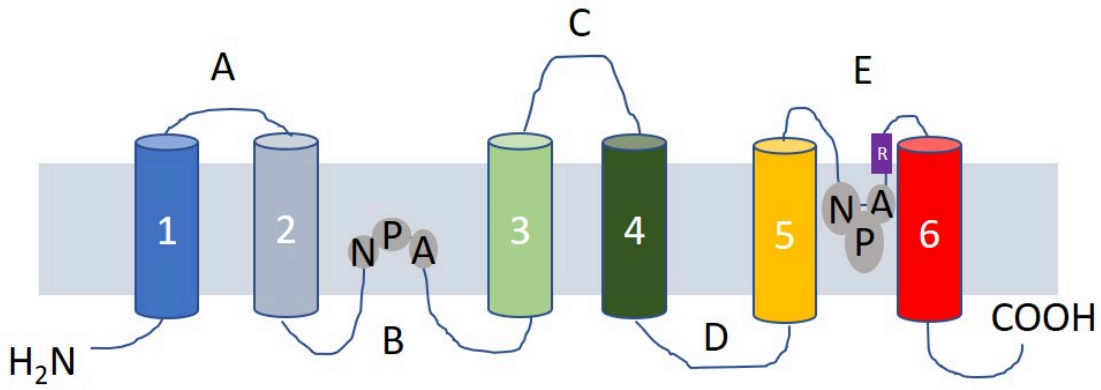

Figure 1.5: The membrane topology of Aquaporins. Reprinted from [72].

helix before it connects with helix transmembrane domain 6 [81], [82].

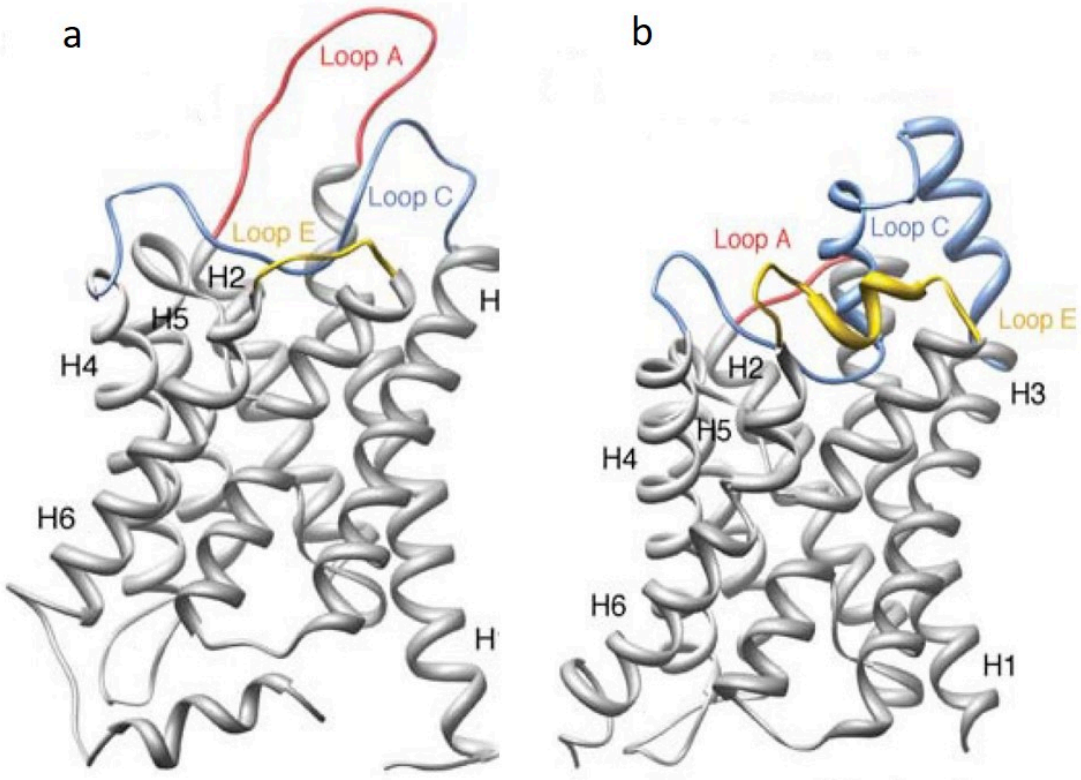

Figure 1.6: A comparison of a) AQP1 and b) GLPF structures in *E. coli*. Taken from [81].

As GLPF's role is to provide more space to transfer glycerol molecules, constriction regions in this type of aquaporin should be larger and also hydrophobic compared to the pores in AQP1 [81], [82]. For example, GLPF has a Phe200 chain which is significantly more hydrophobic than Cys191, and also a Trp48 chain which is larger than Phe58 in AQP1. Besides, GLPF lacks cysteine which leads to less sensitivity to mercurial. These properties form a constriction site with a diameter between $3.8-3.14\mathring{A}$ [70], to permeate glycerol molecules [81], [82].

AQPz and GLPF are considered similar in terms of the amino-acid sequence, although the water permeability of GLPF is estimated at almost one-six of AQPz [81], [85]. It is

interesting to note that it is assumed by other research works that Gram-negative bacteria transfer water and glycerol through to different protein channels, although Gram-positive have a single porin channel which plays a role of water and glycerol channels simultaneously [69].

Water channels intricately woven within the inner lipid membrane of bacteria play a pivotal role in facilitating the transport of water and ions, particularly under hypoosmotic conditions. In this context, the membrane's permeability emerges as a critical factor, further underscoring its significance in regulating cellular processes.

When solutions on either side of a membrane contain varying concentrations of an impermeable solute, water migrates from the side with the lower concentration to the side with the higher concentration. In scenarios involving dilute solutions, the net water flux through a single water channel, denoted as $j_W(\frac{mol}{s})$, exhibits a linear relationship with the solute concentration difference, ΔC_S $(\frac{mol}{cm^3})$ [86].

$$j_W = P_f \Delta C_S \tag{1.1}$$

P_f $(\frac{cm^3}{s})$ is osmotic permeability of the channel which is an indicator of membrane permeability[86], [87]. As per Eq 1.1, the flow of water through the bacterial membrane hinges on two primary factors: the osmotic permeability of the channel and the disparity in solute concentration within the bacterial habitat. This interaction dictates the volume of water transferred across the bacterial cellular structure, contingent upon the channel's water-permeating capabilities and the concentration gradient across the membrane.

Furthermore, this interplay between osmotic permeability and concentration gradient plays a pivotal role in governing water flux into the bacterial membrane, particularly in hypoosmotic scenarios. Given the diverse osmotic permeability exhibited by different water

channels, such as aquaporins within the bacterial membrane, alterations in solute concentration inside and outside the membrane can prompt selective water transfer through these channels based on their unique osmotic permeability characteristics [86].

The concept of bacterial sensitivity to mechanical forces has a long history. As early as 1982, Koch and colleagues [88], proposed a connection between the elongation of individual bacteria and the mechanical stress and strain within the cell envelope associated with turgor pressure. Subsequently, mechanosensitive channels in the bacterial cell membrane highlighted their role in regulating the mechanical deformation [89].

The driving force for opening the protein channels originates from the mechanical deformation of lipid bilayer [90]. As the phospholipid bilayer consists of amphiphilic lipid molecules that possess hydrophilic heads and hydrophobic tails, the obtained tension due to hypoosmotic pressure is accumulated at the neck of the bilayer where the heads and tails are linked to each other [91]. Hence, the surface tension can bend and deform the bilayer, with each embedded protein actively participating in this deformation [90], [91].

On the other side, hydrophobic forces are instrumental in binding the two lipid monolayers of a bilayer, yet these monolayers have the flexibility to slide relative to each other along the bilayer midplane. In processes involving membrane bending, this relative slipping of monolayers often results in a partial relaxation of the overall energy associated with membrane bending [92], [93]. Consequently, the bending deformations of the two membrane monolayers must be separately considered, subject to the constraint of monolayer transverse coupling [94].

Furthermore, the geometric properties of the lipid bilayer are also crucial. One notable geometric characteristic of a lipid monolayer is its thinness, approximately 2 nm, compared to its lateral dimension, which varies from a few hundred nanometers for intracellular vesicles to tens of microns for external membranes of cells or giant liposomes [94]. As a result, the

most comprehensive thermodynamic depiction of a monolayer closely resembles that of a thin interface between two bulk phases, a concept initially formulated by Gibbs in his seminal work "On the Equilibrium of Heterogeneous Substances" [95]. This description involves the Gibbs dividing surface within the monolayer, parallel to the lipid–water interface. The surface is distinguished by the values of extensive thermodynamic parameters such as internal energy, entropy, and masses of the components. Furthermore, it is characterized by geometric properties, specifically the area and two curvatures determined at each point of the dividing surface [94], [96].

Gibbs initially utilized the two principal curvatures, however, it was later recognized that more convenient characteristics for fluid interfaces and laterally fluid lipid membranes are the total curvature and Gaussian curvature [96], [97]. Therefore, the dividing surface can be chosen at any level within the monolayer, with all thermodynamic values depending on this choice [94].

According to Gibbs' formulation of internal energy, energy changes follow the sequence of deformations in a surface and other related parameters such as area, elastic modulus, and curvature [94]. Consequently, researchers have been motivated to explore the relation between the deformation of a surface and its curvature and bending. For this purpose, the classic continuum mechanical model of Helfrich has been widely employed to study the deformation of lipid membranes as the surface [91], [94]. This model considers elastic moduli, mean, and Gaussian curvature and relates these parameters to the energy density of a membrane [91], [97].

In this work, the outcomes of the experimental investigations were leveraged to construct a mathematical model. This model, designed to predict the mechanical responses of the bacterial cell envelope, formulates equilibrium equations elucidating membrane deformations anchored to the meshed structure of peptidoglycan. Consequently, the model yields a set of

nonlinear partial differential equations, effectively addressed through a custom-built Finite Element (FE) scheme. Hence, the overarching objective is to employ a continuum-based model, informed by experimental insights, to anticipate bacterial reactions to hypoosmotic pressure.

The prognostication of bacterial responses in hypoosmotic conditions carries multifaceted implications. It facilitates a nuanced comprehension of bacterial physiology within varied osmotic milieus [98], [99]. The knowledge derived from such investigations holds practical significance, particularly in the realm of biotechnological applications, including but not limited to fermentation [100], and the synthesis of biofuels [101]. The meticulous analysis of how mechanical forces intricately modulate bacterial behavior, accomplished through sophisticated computer simulations and computational inquiries, stands as an imperative endeavor for the refinement and optimization of these intricate processes [98], [99].

For this purpose, we experimentally observed changes in the size of bacteria according to osmotic pressure and, based on the results, attempted to understand the mechanical deformation of Gram-positive bacteria through the classic Helfrich model. As far as the authors know, the mechanical response of Gram-positive bacteria in terms of theory has been overlooked in the related scientific area; however, the Gram-negative group of bacteria, especially *E. coli*, has been extensively studied over the past years.

In 2011, H. Jiang et al. investigated the mechanical properties of *E. coli* in terms of bacterial shape change and focused on the role of peptidoglycan units in cell wall growth [102]. A. Janshoff and C. Steinem described the mechanical properties of a lipid bilayer, such as expansion and bending modulus, in artificial membranes [103]. The volume gradient of *E. coli* under hypoosmotic pressure was studied by exposing *E. coli* to different osmotic conditions and analyzing its behavior through the measurement of volume differences and the relationship between mechanical pressure and solute efflux rate [9]. In addition, A. Boulbitch

et. al proposed a theoretical model, explaining the elasticity of the peptidoglycan as the tension-bearing layer in Gram-negative bacteria. They reported that the glycan strands in peptidoglycan construct a zigzag form, which is associated with the non-linear behavior of bacteria, and studied the relation of bacteria elasticity and the turgor pressure [104].

In Feb 2023, M. Islam et.al predicted cell membrane behavior of *E. coli* under exposure to a nanospike using the finite element method. They modeled the stress and strain relationship as well as bacteria deformation when a nanospike contacted the bacteria surface [105]. H. Hwang et al. simulated cell wall response of *E. coli* due to the surface tension, and calculated compressibility modulus of different layers of *E. coli* cell envelop at different turgor pressure [106]. Besides, D. Jefferies et al. used course-grain molecular dynamics to predict lipopolysaccharide in the outer membrane of Gram-negative bacteria [107].

In July 2023, L. Zhao et.al studied the interaction between *E. coli* cells and nanostructure arrays to understand the mechano-bactericidal mechanism, particularly focusing on hierarchical nanostructure arrays with different heights. Finite element simulations reveal that the critical action sites, where bacterial cells rupture, are consistently at the three-phase junction zone of cell–liquid–nanostructure [108].

Another research group addressed optimal tip sonication settings for temperature-sensitive procedures, such as preparing viable cell extracts. They determined the optimal tip immersion depth to maximize mixing and enhance the thermal dissipation of local cavitation hotspots. A finite element heat transfer model is presented and used to observe the effect of temperature rise on the performance of *E. coli* BL21 DE3 star strain cell extracts [109].

1.6 Objectives and Hypothesis

The primary aim of this research is to bridge the existing knowledge gap concerning bacteria responses to hypoosmotic pressure, with a particular focus on the less-understood behavior of Gram-positive bacteria.

To achieve this overarching goal, the study aims to explore bacterial responses to hypoosmotic pressure with specific objectives, including analyzing Gram-negative and Gram-positive bacteria's reactions. Dynamic light scattering test will quantitatively measure size changes under hypoosmotic conditions, and the study will examine correlations between these changes, external pressure, turgor pressure, and lateral pressure. The mathematical model developed using the Finite Element Method will accurately predict bacteria responses to hypoosmotic pressure. These objectives and the associated hypothesis will guide the experimental and analytical aspects of the research, offering an approach to unraveling the mysteries of bacterial responses to hypoosmotic pressure.

1.7 Thesis Overview

As previously stated, this project focuses on exploring the responses of both Gram-negative and Gram-positive bacteria to hypoosmotic pressure using experimental methods. The obtained data will be employed to predict the response of Gram-positive bacteria through mathematical approaches, solved using the Finite Element Method. The thesis structure is outlined as follows:

- Chapter 2: Materials and methodology.

- Chapter 3: Experimental results on bacteria responses to hypoosmotic pressure, emphasizing size changes and their correlation with external pressure, turgor pressure, and lateral pressure.

- Chapter 4: Mathematical model and Finite Element Method employed in this study, and limitations and future possibilities of this research work.

- Chapter 5: A concise conclusion summarizing key findings of the thesis and future thesis directions.

Chapter 2

Experimental Results

In this study, various solutions were employed to exert hypoosmotic pressure on the bacterial cell envelope, and the response of the bacteria was examined by observing changes in size and deformation through different experimental analysis methods. Additionally, a comparative analysis of both types of bacteria was conducted based on experimental results.

2.1 *L. acidophilus* growth and culturing

L. acidophilus (ATCC 4356) was streaked from a frozen stock at -80 °C on a MRS agar plate, followed by incubating the plates at 37 °C for two days. The bacteria colonies were inoculated in MH broth at 37 °C in an incubator (Innova 42 incubator shaker, Edison, NJ) anaerobically overnight. *L. acidophilus* was centrifuge-washed twice in Phosphate-buffered saline (PBS) and one time in DI water for 10 minutes at 11,000 rpm. The optical density of about $10^8 - 10^9$ cell/ml was obtained for the cultured *L. acidophilus*.

2.2 *E. coli* growth and culturing

E. coli (ATCC 25922) was cultured from a frozen stock at -80 °C in MH broth. The process involved several culturing steps. Initially, the bacteria were streaked on an MH agar plate, followed by overnight incubation at 37 °C. Subsequently, a single bacterial colony was inoculated in MH broth and cultured at 37 °C and 200 rpm in an incubator. The next day, the bacterial suspension was transferred into the fresh medium at a 1:100 ratio and grown at 37 °C and 200 rpm for 4 hours. *E. coli* was washed twice in PBS and once in DI water using a centrifuge (Eppendorf 5804R, Hamburg, Germany) for 10 minutes at 11,000 rpm. Approximately 3×10^9 cells/ml was obtained for the cultured *E. coli*.

2.3 Hypoosmotic shock

The samples from both bacteria groups were osmotically shocked by adding a 0.9% (w/v) saline solution, which was then diluted to 0.45% and 0.22% (w/v) to have three hypoosmotic conditions. The hypoosmotic pressures provided through these salt solutions were measured using a Vapor Pressure Osmometer (VAPRO, Model 5600) at 300 mOsmol/l (mOsm), 150 mOsm, and 75 mOsm, respectively.

Additionally, DI water (0 mosM) was added to the samples to compare bacterial responses under different hypoosmotic pressures. A brief schematic of culturing the cells and applying hypoosmotic pressure is shown in Figure 2.1.

2.4 Dynamic Light Scattering (DLS) test

To examine how bacteria respond to hypoosmotic pressure, particularly in terms of changes in size, we conducted the dynamic light scattering (DLS) test (DLS machine, ALV/CGS-3 Goniometer) at 22 °C. DLS measures brownian motion of the particles in a solution. DLS technique provides information about the size distribution and diameter of the bacteria. In this research work, the bacteria samples were introduced to the DLS machine approximately 15 minutes after the down-shock, and the test was performed on all samples.

2.5 Transmission Electron Microscopy (TEM) test

Transmission Electron Microscopy was used to capture morphological changes of bacteria under exposure to hypoosmotic pressure. The test was performed using the TEM at 20 KV (JEOL JEM 2100; Peabody, MA). Besides, bacteria samples were negatively stained using 1.5 w/v phosphotungstic acid hydrate at pH 7.0 (Sigma-Aldrich).

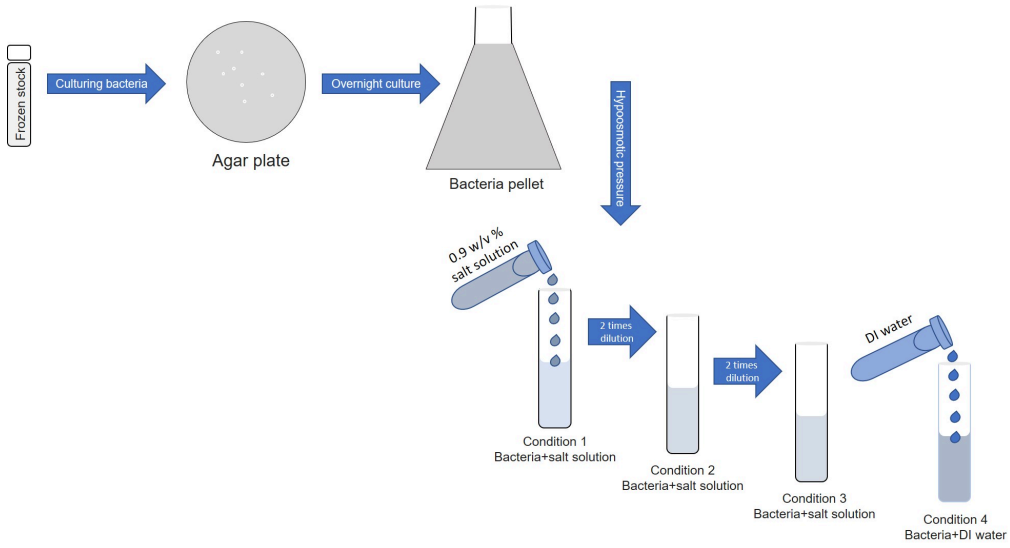

Figure 2.1: The process of adding different salt solutions and DI water to bacteria pellet.

Following the bacterial culturing process, we examined the impact of hypoosmotic pressure on bacterial colonies by assessing changes in morphology.

2.6 Study of Size changes by DLS test

The DLS results are shown in Figure 2.2, indicating the size change of each group of bacteria in response to four different osmolarity conditions. The diameter values, obtained from the DLS test, are also presented in Table 2.1.

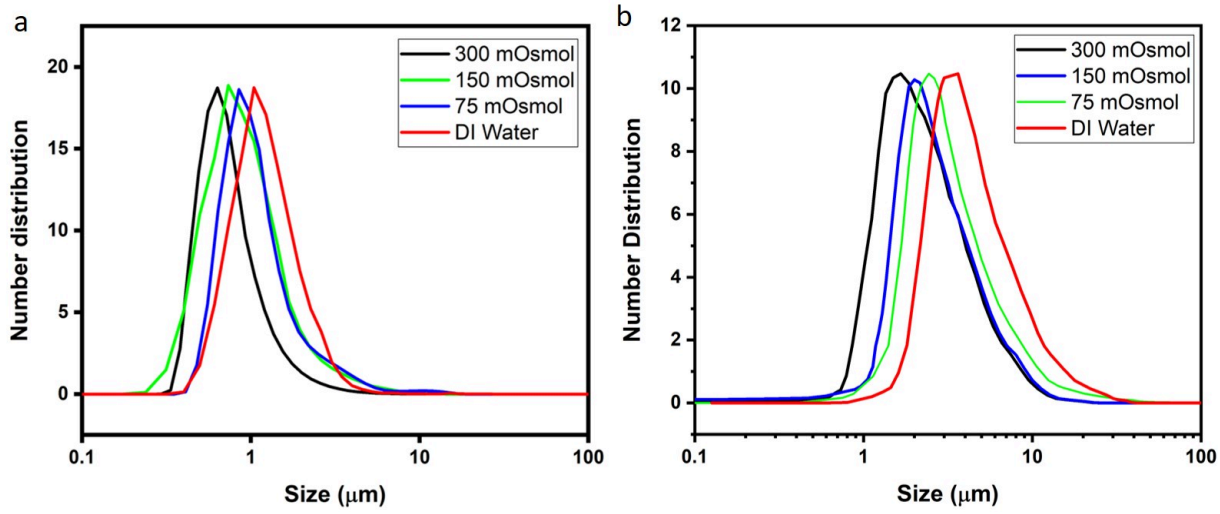

Figure 2.2: DLS test results of a) *E. coli*, b) *L. acidophilus*.

By subjecting bacteria to hypoosmotic conditions, they undergo a series of three distinct response phases. Initially, immediately following the introduction of hypoosmotic conditions, bacteria undergo swelling and extension, transitioning from their initial morphology to an expanded state. Subsequently, bacteria tend to counteract the applied pressure, endeavoring to revert to their equilibrium state. In this phase, they actively respond to the applied pressure by employing water channels. Finally, as bacteria respond to the pressure by releasing excess solute and facilitating water influx, they ultimately return to their equilibrium

Osmolarity (mOsm)	*E. coli* (μm)	*L. acidophilus* (μm)
300	0.904±0.016	1.63±0.11
150	1.038±0.024	1.91±0.13
75	1.179±0.021	2.44±0.23
0	1.348±0.037	3.58±0.24

Table 2.1: Diameter results of both *E. coli* and *L. acidophillus* from the DLS test.

state and regain their original morphological shape. The reported DLS test results were acquired after the application of hypoosmotic pressure, capturing the expansion of bacteria in response to the downward shock.

Figure 2.3 delineates alternations in the size of both *E. coli* and *L. acidophilus* as the osmolarity diminishes along the hypoosmotic gradient from 300 mOsm to 0 mOsm, attained by DI water. Notably, *L. acidophilus* undergoes a more pronounced size change compared to *E. coli* under varying osmolarity conditions of 300, 150, 75, and 0 mOsm.

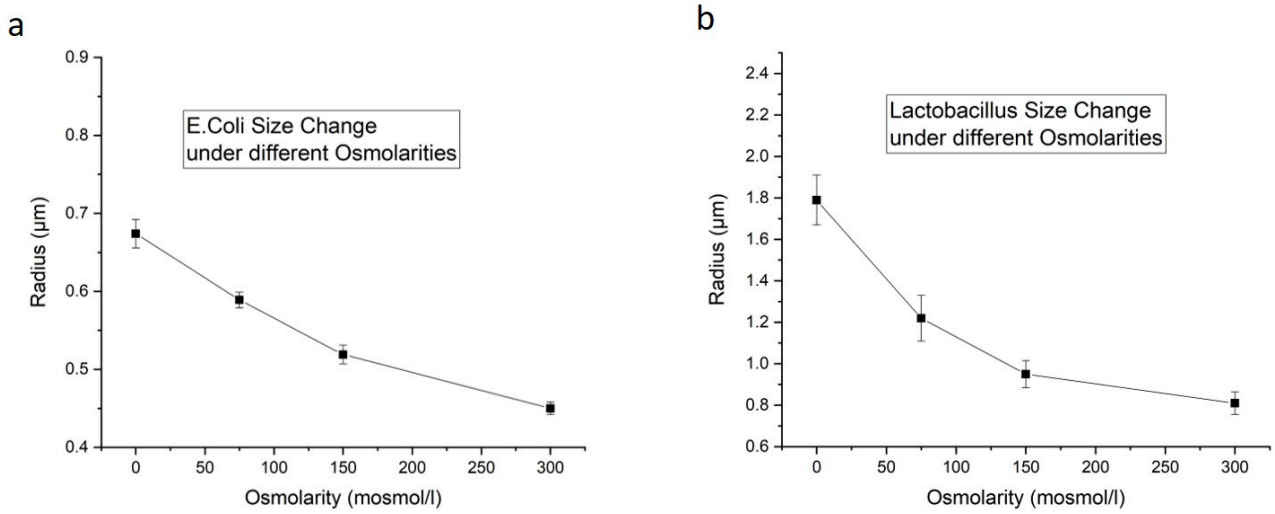

Figure 2.3: Bacteria size change under different osmolarities. a) *E. coli*, b) *L. acidophillus*.

This augmentation in size precipitates swelling and elongation in both bacterial types, resulting in an expanded radius of the bacteria. Additionally, the outcomes reveal that the maximum radius is achieved by introducing DI water (0 mOsm) to *L. acidophilus* bacteria

cells, reaching approximately 1.79±0.06 μm. Furthermore, the reduction of extracellular osmolarity from 300 mOsm to 0 mOsm prompts a 26.1% volume increase in *L. acidophilus*, in contrast to *E. coli*, which experiences a mere 3% volume increase.

2.7 Study of external pressure on bacteria

Incorporating various solutions with distinct solute concentrations introduces diverse external pressures on bacteria, as depicted in Figure 2.4.

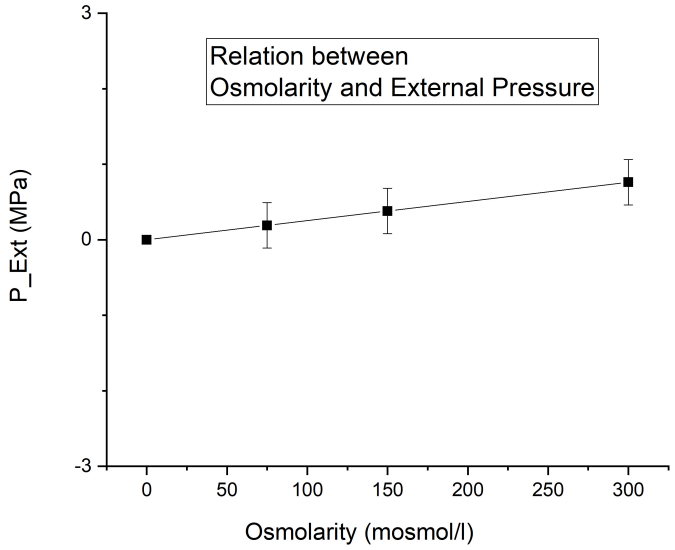

Figure 2.4: Change of external pressure by applying different osmolarities.

The osmolyte solution, delivering an osmolarity of 300 mOsm, exhibits a higher solute concentration in contrast to DI water, which has 0 mOsm, consequently yielding a higher external pressure. By adding the solution of 300 mOsm, an external pressure of about 0.76 MPa is applied on the bacteria, in stark contrast, no external pressure is provided by DI water with 0 mOsm.

2.8 Study of turgor and lateral pressure on bacteria

Prior scientific studies have documented the emergence of differences in extracellular and intracellular concentrations in both Gram-negative and Gram-positive bacteria when subjected to various solutions. This phenomenon is elucidated by the equation proposed by Wennerström et al [110], which aims to comprehend and explore the absolute value of Turgor pressure within bacteria. Turgor pressure arises as a consequence of the solute concentration gradient between the interior and exterior of the bacterial cell. Figure 2.5 provides a schematic depiction of Turgor pressure acting on the inner membrane.

$$P_{Turgor} = P_{mol} - P_{ext} \tag{2.1}$$

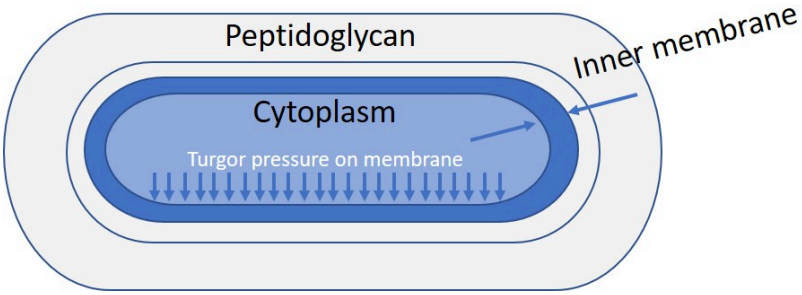

Figure 2.5: Turgor pressure is applied on inner membrane inside the bacteria as a result of solute gradient.

Given the notably substantial size changes observed in Gram-positive bacteria when exposed to various salt solutions, we elected to focus on Gram-positive type for further investigation. To delve into this, alterations in turgor pressure, contingent on intracellular and extracellular pressure (as per Eq. 3.1), are illustrated in Figure 2.6 specifically for *L. acidophilus* bacteria.

With the elevation of external pressure, signifying an increase in external osmolarity, bacteria undergo a decline in turgor pressure owing to the diminished gradient between

internal and external solute concentrations. The 0.76 MPa difference in external pressure, stemming from the solution with 300 mOsm and DI water with 0 mOsm, results in a turgor pressure difference of 0.63 MPa. The solute concentration and internal pressure within Gram-positive bacteria are documented to be approximately 0.3 Molar and 7 bar, respectively. The exerted turgor pressure contributes to both tension and lateral pressure, inducing stretching in the bacteria's cell wall [110]. As the cell wall expands, the assumption is made that the bacteria's shape is nearly transforming to spherical when exposed to salt-water solutions. The relationship between these two pressure variables is delineated by incorporating parameters of radius (R) and thickness (h), as the absolute value of lateral pressure, as defined in [12]. The radius values are considered based on the DLS test, and the thickness is also assumed to be 50 nm based on the research papers [12].

$$P_{Lat} = (P_{Turgor})R/2h \tag{2.2}$$

To this end, alterations in applied lateral pressure on *L. acidophilus* due to varying hy-

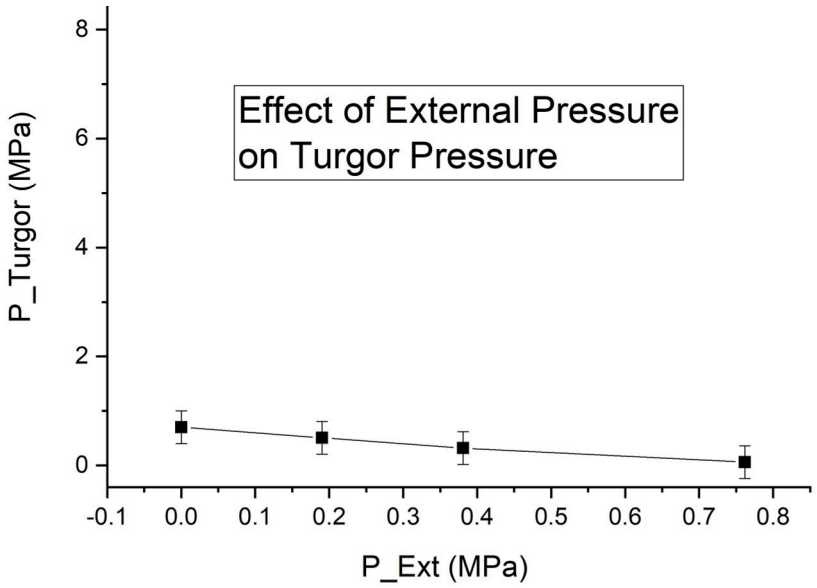

Figure 2.6: Change of Turgor pressure in different external pressures.

poosmotic pressures are depicted in Figure 2.7. Additionally, the relationship between turgor pressure and lateral pressure is illustrated. As evident, the increase in the radius of bacteria from 0.81±0.05 μm to 1.79±0.06 μm, obtained by introducing a solution of 300 mOsm and DI water with an osmolarity of 0 mOsm, corresponds to *L. acidophilus* experiencing turgor pressures of 0.061 MPa and 0.7 MPa, respectively. This upward trajectory aligns well with the change in lateral pressure concerning the augmented radius of bacteria.

Enhanced expansion, attributed to elevated turgor and lateral pressure, results in substantial swelling of the bacteria and an increased radius. Figure 2.7 further illustrates the alteration in lateral pressure due to variations in turgor pressure within the bacteria. It is evident that heightened turgor pressure, stemming from the addition of a solution with lower solute concentration, imposes greater tension on the bacteria cell wall, consequently resulting in an augmented lateral pressure.

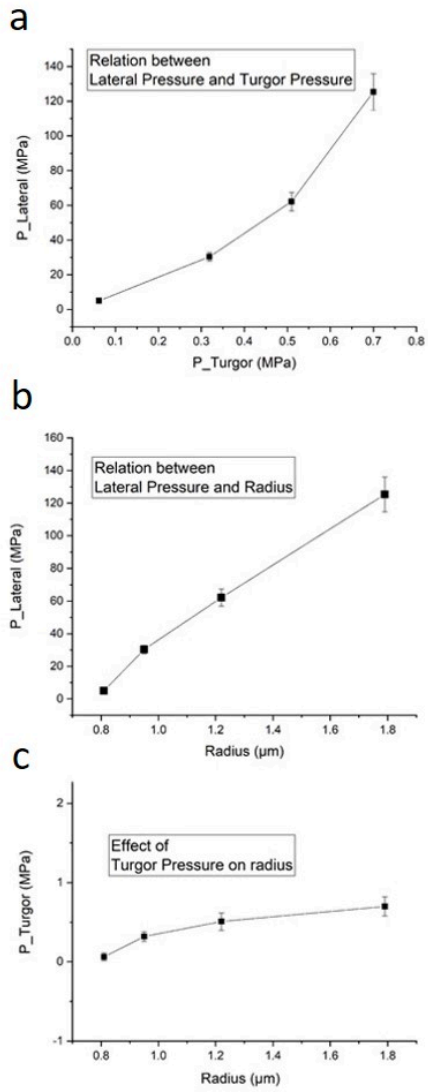

Figure 2.7: The relation between a) lateral and turgor pressure, b) radius and lateral pressure, and c) radius and Turgor pressure on bacteria.

Chapter 3

Theoretical Results

As previously highlighted, the preference for predicting mechanical responses in Gram-positive bacteria, as opposed to Gram-negative, is rooted in the limited theoretical exploration of shape deformation in Gram-positive bacteria under hypoosmotic pressure [9], [102]–[107].

3.1 Mathematical Model

To comprehend the alterations in bacteria size, it is crucial to delve into the mechanical responses of the cell envelope under the impact of turgor and lateral pressure. The adjustment of applied pressure significantly influences the energy equilibrium within the cell wall assembly. Consequently, the energy change is intricately linked to variations in specific mechanical parameters as the bacteria undergo deformation under pressure in comparison to their undeformed state before pressure application. These states are respectively regarded as the current and reference configurations. Numerous models to investigate the mechanical behavior of bacteria cells have been used over the past decades [97], [111].

The very first models related to strain energy functional of red blood cells were proposed by Canham [111], and developed by Helfrich [97], to study shape deformation of lipid bilayers of the cells when some parameters such as pressure and volume change.

Helfrich, acknowledging that a lipid bilayer constituting cell membranes is in a liquid crystal state [112], conceptualized a membrane as a 2D smooth surface in a 3D Euclidean space due to its significantly smaller thickness compared to its lateral dimension. Drawing an analogy with the Frank energy of a bent nematic crystal box [113], Helfrich introduced the curvature energy per unit area of the membrane. He also incorporated spontaneous curvature into his model, signifying the asymmetry between the two layers of the membrane. Following this, Canham developed another model, considered a special case of Helfrich curvature energy when the spontaneous curvature is zero [112].

A few years later, a bilayer-coupled model was developed to generalize the stomatocyte–discocyte–echinocyte transition in human red blood cells, utilizing the Helfrich model. When a lipid bilayer undergoes bending from a flat configuration, the area per lipid molecule in each leaf deviates from the equilibrium value. To account for the in-plane stretching and compression in each leaf, a nonlocal term that contains the compression modulus and the thickness of the monolayer was introduced to the bending energy of membranes [112], [114]. Besides, in 1988, Helfrich and Prost posited that chiral molecules in chiral membrane structures remain in the phase where the orientation of molecules is consistently tilted from the normal of membranes at a constant angle. They selected a locally right-handed orthogonal frame n, m, p, with n representing the normal vector of the membrane, m denoting the projection of the tilting direction on the membrane, and p coinciding with the axis of ferroelectric polarization and studied membrane bending and its energy [115].

Based on Helfrich and Prost's model, Ou-Yang and Liu studied a transition sequence from vesicle to twisted ribbon, and ultimately to a helical stripe [112]. Moreover, Selinger

and Schnur formulated the Helfrich–Prost model to describe chiral lipid tubules, predicting the existence of a tubule with a helically modulated tilting state. The model's free energy incorporates three main contributions: curvature free energy, tilting free energy, and the Frank free energy [116].

The classic Helfrich energy equations are mostly employed to investigate elastic bending energy which is stored in the membrane and its components. This analysis provides some differential equations defined on certain shapes and geometry of the cell membrane through principles for minimization of the Helfrich energy functional. The obtained equations have some parameters that require numerical and computational study to solve them and find the results in terms of membrane deformation. The simulated model contains the partial differential equations (PDEs) which define the shape deformation of cell [117].

In our proposed model, the deformation of Gram-positive bacteria, which possess a cell envelope containing an inner membrane and peptidoglycan, is studied over Gram-negative ones with an extra layer of outer membrane. As Gram-positive bacteria contain an assembly of inner membrane-peptidoglycan and these layers respond to pressure through morphology changes that originate from mechanical properties, therefore, the obtained deformation in the cell wall is related to the lipid membrane bending energy, and also extension, bending, and twist energy in peptidoglycan.

The model considers the peptidoglycan as a mesh-like structure attached to the inner membrane through several proteins. It is assumed that these layers respond to hypoosmotic pressure through their bending, extension, and twist. We used the following equation to study the effects of hypoosmotic pressure on Gram-positive type [97].

$$W = kH^2 + \bar{k}K + \frac{1}{2}E_1\varepsilon_1^2 + \frac{1}{2}E_2\varepsilon_2^2 + \frac{1}{2}C(\mathbf{g_1}\cdot\mathbf{g_1} + \frac{1}{2}\mathbf{g_2}\cdot\mathbf{g_2}) + \frac{1}{2}D\mathbf{g_1}\cdot\mathbf{g_2} \tag{3.1}$$

where H is the Mean curvature, K is the Gaussian curvature, k and k^{-} are bending modulus which is an intrinsic property of inner membrane and is mostly dependent on the composition of lipid bilayers in bacteria, E is the Young's modulus, g_1 and g_2 are geodesic curvature, C and D are bending and twist stiffness, respectively.

According to this equation, the strain energy of the lipid membrane and peptidoglycan in Lactobacillus is defined based on the relation between the Mean and Gaussian curvature of the membrane (the first two terms), strain energy (the second two terms) as well as bending and twist in peptidoglycan layer (the last two terms). The last two terms describe how other components such as glycan and peptides in peptidoglycan are curved in response to deformation in membrane-peptidoglycan assembly.

Since the Helfrich model assumes a lipid membrane as a thin shell, therefore, mathematical relations in surface geometry matter. Besides, it assumes the membrane as a two-dimensional surface that is embedded in a three-dimensional Euclidean space [90]. In this case, thickness is trivial compared to other dimensions. The curvature energy per unit area of a membrane is defined by the first two terms in Eq. 3.1, which assumes a membrane as a symmetric lipid bilayer consisting of two monolayers with zero spontaneous curvature [112].

In addition, the relation between principles curvatures C_1 and C_2 defines Mean and Gaussian curvature. Principle curvatures C_1 and C_2 are the maximum and minimum curvature of a curved surface, with respect to R_1 and R_2 as the radius of the curvature, respectively [91].

$$H = C_1 + C_2$$

$$K = C_1 C_2$$

$$C_1 = 1/R_1$$

$$C_2 = 1/R_2$$

When a bacteria cell is exposed to hypoosmotic pressure, it experiences shape change and it tends to adopt an equilibrium shape in which the total Helfrich curvature energy is minimal. This energy is obtained by the integration of parts on terms in Eq. 3.1 [112]. By changing a system's shape, the energy of the system also changes which emphasizes the necessity of shape variations understanding. For this purpose, calculation of the variation of the energy and its parameters is essential to analyze energy minimization of bacteria cell envelope.

First, we introduce $r(\theta^\alpha)$ which is the equilibrium position of a point in a three-dimensional space with respect to the coordinates θ^α, and also virtual displacement $u(\theta^\alpha) = \dot{r}$ [118]. This superposed dot signifies the derivative concerning a specific parameter. Besides, displacement is defined as the relation between tangential (u^α) and normal (n) variations [118].

$$\mathbf{u} = u^\alpha \mathbf{a}_\alpha + u\mathbf{n}$$

As the energy density based on the Helfrich model (Eq. 3.1) is a function of Mean and Gaussian curvature, terms of H and K need to be explained [118].

$$H = \frac{1}{2} a^{\alpha\beta} b_{\alpha\beta}, K = \frac{1}{2} \varepsilon^{\alpha\beta} \varepsilon^{\lambda\mu} b_{\alpha\lambda} b_{\beta\mu}$$

There are different terms in these equations which need to be defined. The term $a^{\alpha\beta}$, as the inverse of the metric tensor $a_{\alpha\beta}$, is the matrix of the contravariant metric tensor [118].

The term $b_{\alpha\beta}$ is the component of the second fundamental form [118]. In other words, it is defined as the covariant component of the surface curvature tensor. As for the Gaussian curvature components, $\varepsilon^{\alpha\beta}$ is the permutation tensor density, defined as $\varepsilon^{\alpha\beta} = e^{\alpha\beta}/\sqrt{a}$ where

$a = det(a_{\alpha\beta})$ [118]. The other term that needs to be defined is the contravariant cofactor of the curvature $\varepsilon^{\alpha\lambda}\varepsilon^{\beta\gamma}b_{\lambda\gamma} = \tilde{b}^{\alpha\beta}$ [118].

By substituting this to Gaussian curvature equation, we have the following relation [118].

$$b_{\mu}^{\beta}\tilde{b}^{\mu\alpha} = Ka^{\beta\alpha}$$

The relation between these components is defined based on the Gauss and Weingarten equations, respectively, as follows [118].

$$\mathbf{a}_{\alpha;\beta} = b_{\alpha\beta}\mathbf{n}$$

$$\mathbf{n}_{,\alpha} = -b_{\alpha}^{\beta}\mathbf{a}_{\beta}$$

According to these equations, we introduce $a_{\alpha\beta} = a_{\alpha}.\beta$ (this dot is defined as Euclidean inner products on 3-D space) where $a_{\alpha} = r_{,\alpha}$ are the tangent vectors and $n(\theta^{\alpha}) = \frac{1}{2}\varepsilon^{\alpha\beta}a_{\alpha} \times a_{\beta}$ is the vector field for normal vector [118]. In addition, semi-colon notation in the Gauss equation refers to the differentiation of surface covariant. Therefore, the relation between covariant differentiation and partial differentiation is denoted by the Christoffel symbol on ω as the surface, as follows [118].

$$\mathbf{a}_{\alpha;\beta} = \mathbf{a}_{\alpha,\beta} - \Gamma_{\alpha\beta}^{\lambda}\mathbf{a}_{\lambda}$$

Through the explained relations, we define the equilibrium state of the cell membrane by the energy potential of the membrane [118].

$$E = \int_{\omega} W(H, K; \theta^{\alpha}) da \tag{3.2}$$

This equation is equipped by some other terms such as Lagrange multiplier of $\lambda(\theta^{\alpha})$ and A which is the value of a on reference surface of Ω in equation $J = \sqrt{\frac{a}{A}}$. This modification is done to apply constraints on the area [118].

$$E = \int_{\Omega} [JW(H, K; \theta^{\alpha}) + \lambda(\theta^{\alpha})(J-1)] dA \tag{3.3}$$

Recalling the energy variation, we equip this equation with the explained terms as follows [118].

$$\dot{E} = \int_{\omega} [\dot{W} + (W + \lambda)\dot{J}/J] da \tag{3.4}$$

$$\dot{W} = W_H \dot{H} + W_K \dot{K}$$

where $W_H = \partial W/\partial H \quad and \quad W_K = \partial W/\partial K$ as the partial derivatives [118]. When it comes to the terms of energy variation equation, they are defined as [118]

$$\dot{W} = u^{\alpha}(W_H H_{,\alpha} + W_K K_{,\alpha})$$

$$(W + \lambda)\dot{J}/J = [(W + \lambda)u^{\alpha}]_{;}\alpha - u^{\alpha}(W + \lambda)_{,\alpha} \tag{3.5}$$

where

$$\dot{J}/J = u^{\alpha}_{;\alpha}$$

$$\dot{H} = u^{\alpha}H_{,\alpha} \quad and \quad \dot{K} = u^{\alpha}K_{,\alpha}$$

By substituting the above equations into the energy variation equation, the tangential framework yields to [118]

$$\dot{E} = \int_{\omega} u^{\alpha}(W_H H_{,\alpha} + W_K K_{,\alpha} - W_{,\alpha} - \lambda_{,\alpha})da + \int_{\partial\omega} (W + \lambda)u^{\alpha}v_{\alpha}ds \tag{3.6}$$

v_{α} in this equation is defined as the covariant components of the unit normal to the boundary $\partial\omega$. According to [119], the following terms are obtained for normal framework.

$$\dot{J}/J = -2Hu$$

$$2\dot{H} = \Delta u + u(4H^2 - 2K)$$

$$\dot{K} = 2KHu + (\tilde{b}^{\alpha\beta}u_{,\alpha})_{;}\beta$$

In the above equation, the following term is defined as the Beltrami operator,

$$\Delta(.) = a^{\alpha\beta}(.)_{;\alpha\beta}$$

considering these terms, we rewrite the potential energy variation,

$$(W + \lambda)\dot{J}/J$$

then, the following equation is obtained as a normal variation framework.

$$\dot{E} = \int_{\omega} u[\Delta(\tfrac{1}{2}W_H) + (W_K)_{;\beta\alpha}\tilde{b}^{\beta\alpha} + W_H(2H^2 - K) + 2KHW_K - 2H(W + \lambda)]da + \tag{3.7}$$

$$\int_{\partial\omega}[\tfrac{1}{2}W_H v^{\alpha}u_{,\alpha} - (\tfrac{1}{2}W_H)_{,\alpha}v^{\alpha}u + W_K\tilde{b}^{\alpha\beta}v_{\beta}u_{,\alpha} - (W_K)_{,\alpha}\tilde{b}^{\alpha\beta}v_{\beta}u]ds$$

For expanding the energy variation equation, $W_{,\alpha}$ needs to be defined [118],

$$W_{,\alpha} = W_H H_{,\alpha} + W_K K_{,\alpha} + \frac{\partial W}{\partial \theta^{\alpha}} \tag{3.8}$$

As the referred Helfrich model [97], in this study work does not consider the bending and twist of the peptidoglycan layer, we modified the above equation to include terms related to these two properties.

$$W_{,\alpha} = W_H H_{,\alpha} + W_K K_{,\alpha} + W_{\varepsilon}\varepsilon_{,\alpha} + W_{g\cdot}g_{,\alpha} + \frac{\partial W}{\partial \theta^{\alpha}} \tag{3.9}$$

By doing some algebra, the variational work of W is balanced by virtual load P and finally normal shape equation which describes inner membrane-peptidoglycan assembly is obtained as follows. From the chemical viewpoint, as the bacteria always try to recover to the original shape and energy level and stay in mechanical equilibrium, it means that the work which is done by pressure is equal to strain energy change through the structure [102].

$$\begin{aligned}\Delta(\tfrac{1}{2}W_H) + (W_K)_{;\beta\alpha}\tilde{b}^{\beta\alpha} + W_H(2H^2 - K) + 2KHW_K - 2H(W + \lambda) \\ -\tfrac{E_1}{2}Q - \tfrac{E_2}{2}R + C[S] + C[T] + \tfrac{D}{2}[Y] + \tfrac{D}{2}[Z] = P\end{aligned} \tag{3.10}$$

where Q, R, S, T, Y, and Z are explained as the equations that implicate extension, bending, and twist in the peptidoglycan layer, respectively. These terms are expanded in the Supplementary information section.

Chapter 4

Numerical Results

4.1 Finite Element Method (FEM)

Within the engineering domain, the construction of models stands as a foundational activity, playing a pivotal role in achieving solutions that strike a balance between computational efficiency and simulation accuracy. The progression of this process, transitioning from manual computations and simplified models to contemporary high-fidelity simulations executed on powerful computing systems, mirrors the ongoing advancement in engineering tools and technology [120].

Given the intricate nature of biological systems, there is a continual demand for sophisticated computational models. These models play a crucial role in offering a comprehensive understanding of biological systems. They facilitate accurate predictions and evaluations of hypotheses which contribute to advancing scientific knowledge in the field. For this purpose, researchers can leverage these models to enhance their insights and deepen their understanding of the complexities inherent in biological systems. Extensive research in the past decades [121], [122], has delved into the examination of computational models focusing on biological

cellular structures. Among these models, continuum approaches emerge as widely adopted methodologies for the modeling of cellular structures within biological systems [104], [105]. These approaches, rooted in mathematical methods, conceptualize cellular structures as continuous and deformable materials. In particular, the Finite Element Method, a prominent continuum approach, intricately dissects intricate problems into a finite set of interconnected elements. These elements are treated as continuous and deformable entities, enabling a holistic analysis of the material's behavior through the examination of these elements [104], [105], [121], [122].

The Finite Element Method (FEM), acknowledged as one of the most potent and successful numerical analysis techniques, has experienced widespread adoption since the 1950s. Its origins can be traced back to Turner's introduction of the direct stiffness method for structural design in the aerospace industry [122]. Over the subsequent decades, FEM has attracted considerable attention from scientists and evolved into a powerful tool for addressing engineering challenges. Its versatile applications extend across various domains, encompassing structural and mechanical engineering, material science, and biomechanics, solidifying FEM as an indispensable solution for a diverse array of engineering problems [122].

To elucidate the correlation between applied pressure and bacterial deformation as per the derived mathematical model, we leveraged finite element analysis. This computational technique enables the prediction of bacterial behavior under hypoosmotic pressure. The numerical solver utilized to address the governing equations was the Newton-Raphson method, seamlessly integrated into the FENICS platform—a Python-based solver accessible as open-source software. Bacteria cultured in a medium with diverse chemical compound ratios and exposed to varying physical parameters, such as temperature, exhibit distinct mechanical properties, including variations in Young's modulus [7], [123]–[125].

In this simulation, lateral pressure is determined according to experimental data (Figure

3.6). Obtaining precise numerical solutions in the Finite Element Method involves addressing nonlinearities in the governing equations. Despite the complexities in the analytical model equations, the Finite Element Method simulation yields a reasonable deformation profile in response to changes in parameters. To tackle these nonlinearities and guarantee the convergence of our numerical solutions, we utilized the established Newton-Raphson method alongside Galerkin discretization to discretize the problem. This iterative technique is crucial in refining our Finite Element Method (FEM) simulations and improving the accuracy of our results. A concise overview of the FEM simulation is presented in Figure 4.1, illustrating the procedure of applying a FEM model with approximation to a problem. The iteration persists until the convergence reaches a predefined level of tolerance.

The captivating dynamics of the iterative solver's convergence in our Finite Element Method (FEM) simulation are vividly illustrated in Figure 4.2. This iterative process is a pivotal aspect of our computational model, offering valuable insights into the gradual refinement of the solution. The figure encapsulates the outcomes of the iterations, presenting the evolution of the solution as the iterative solver approaches convergence with the true solution.

The convergence of the iterative solver serves as a testament to the efficacy of our model in approximating the desired solution. The iterative process unfolds as a stepwise journey, where with each iteration, the solution progressively converges towards the true solution. The figure visually represents this convergence, highlighting the reduction in the residual with increasing iterations. The residual is defined as a measure of the solution's deviation from the true solution.

The diminishing trend of the residual, approaching zero as iterations progress, is a compelling indicator of the solver's convergence. The residual trends emphasize how out-of-plane deformation prediction deviates from the true solution for different pressure values. In prac-

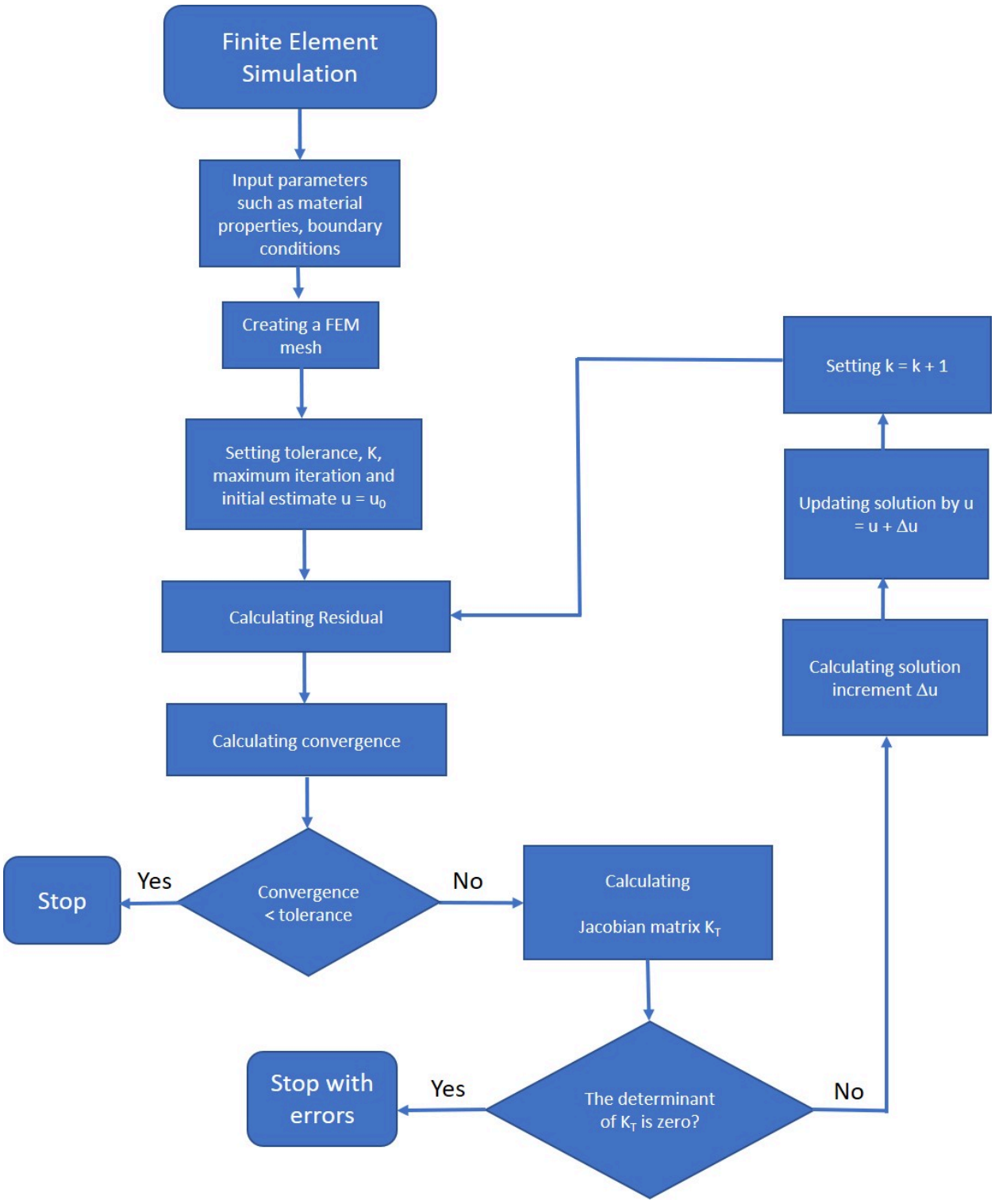

Figure 4.1: A chart of Newton Raphson approach used in Finite Element Method .

tical terms, this signifies that the solution is systematically getting closer to the accurate solution as the iterative process unfolds. The diminishing residual values underscore the model's capacity to iteratively refine its predictions, thereby providing a reliable and convergent solution to the complex problem at hand. This iterative convergence not only enhances the accuracy of our predictions but also instills confidence in the reliability of the FEM simulation as a robust computational tool for studying the mechanical responses of the system under investigation.

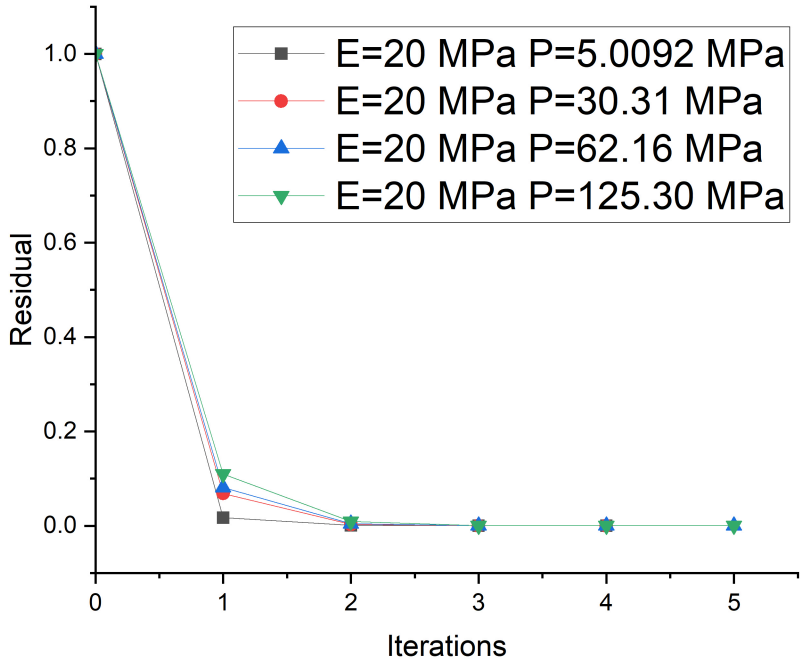

Figure 4.2: The relation between the increased number of iterations and residuals, emphasizing how out-of-plane deformation prediction deviates from the true solution by increasing the residuals.

4.2 Discussion

In the theoretical model, the impact of hypoosmotic pressure on Gram-positive bacteria deformation and displacement is investigated. For this model, Young's modulus of 20 MPa is assumed, as commonly reported for Gram-positive bacteria, specifically the Bacillus type [7], [124], [125]. Figure 4.3 illustrates the initial state of the simulation, incorporating a mesh of triangular elements in a 2-D domain.

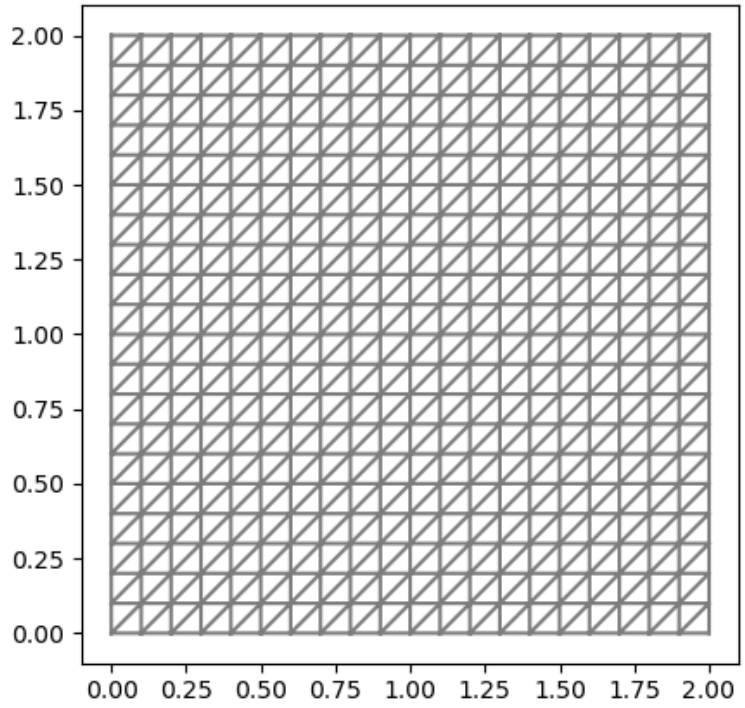

Figure 4.3: A mesh of triangular elements in a 2x2 configuration used in Finite Element Method. The dimension is normalized by the surface configuration.

The proposed model, conceptualizing the Gram-positive cell envelope as a thin shell, intricately explores the dynamics of in-plane deformation inherent in this structure, as showcased in Figure 4.4. The figure offers a detailed portrayal of the nuanced responses exhibited under different pressures. It illuminates the dimensionless in-plane deformation, a pivotal aspect of structural behavior, to reveal the subtle adjustments and adaptations occurring within the Gram-positive cell envelope. The figure captures the intricate interplay between the thin shell structure and the applied pressures, providing a visually comprehensive representation of the model's predictions across a range of pressure conditions.

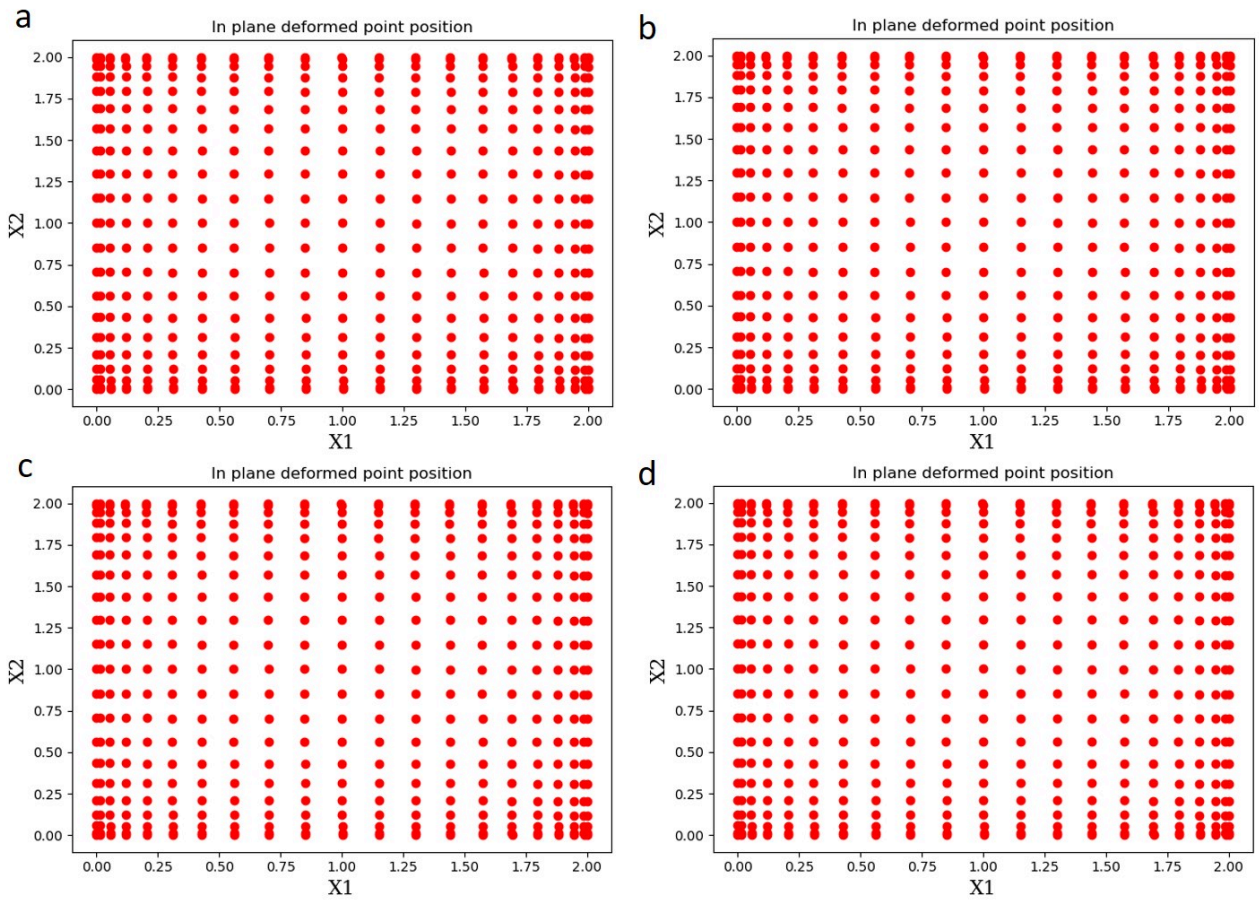

Figure 4.4: In-plane deformation a) $P_{lat} = 5$, b)$P_{lat} = 30.31$, c) $P_{lat} = 62.16$ and d)$P_{lat} = 125.30$ MPa which is normalized by the surface configuration.

Our postulation that the Gram-positive cell envelope primarily deforms in the Z direction under applied pressure is visually depicted in the meticulous presentation of out-of-plane deformation in Figure 4.5. This representation comprehensively illustrates the dynamic response of the thin shell structure to varying pressure conditions. Significantly, the figure reveals a discernible and consistent upward trend in deformation as the applied pressure increases. This observed trend aligns seamlessly with findings from analogous studies on Gram-positive bacteria, as discussed by Rui Han et al. [126].

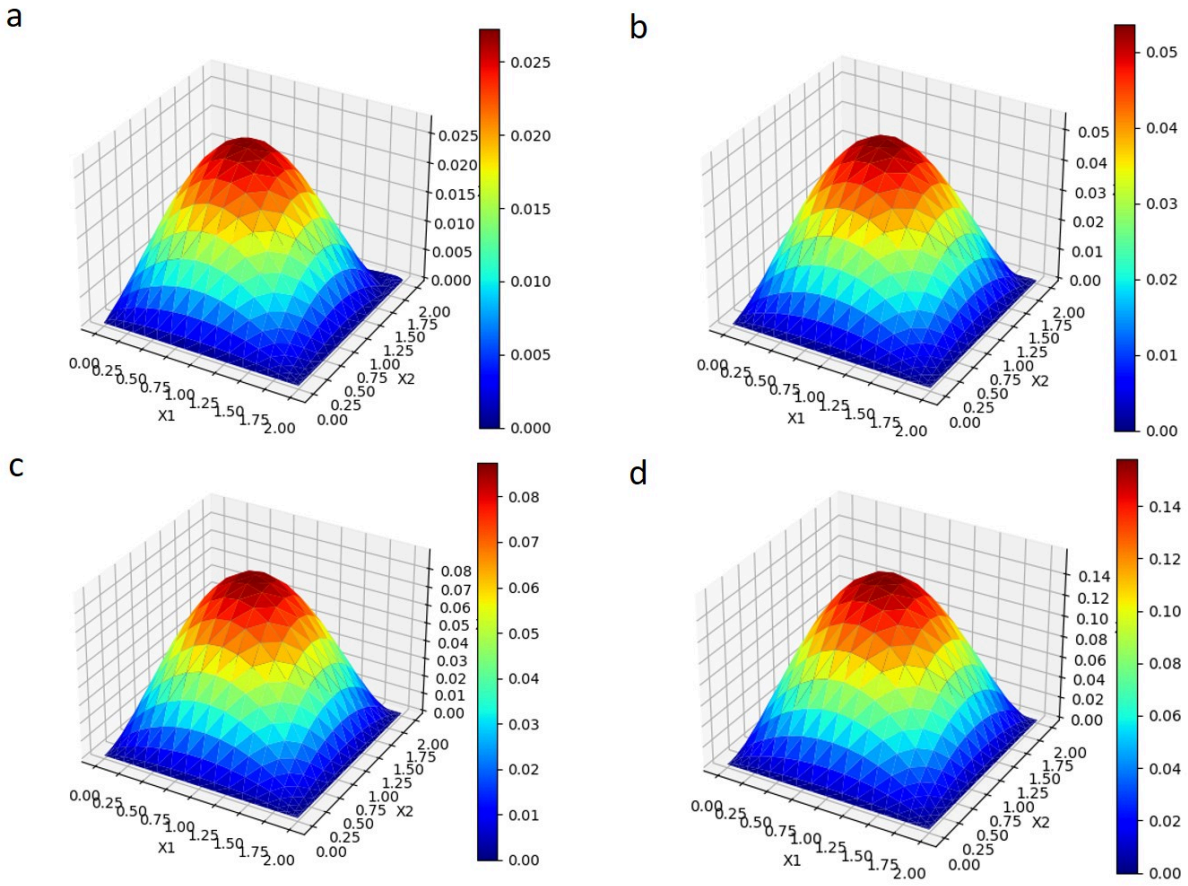

Figure 4.5: Out-of-plane deformation a) $P_{lat} = 5$, b)$P_{lat} = 30.31$, c) $P_{lat} = 62.16$ and d)$P_{lat} = 125.30$ MPa which is normalized by the surface configuration.

Essentially, the model anticipates a substantial increase in deformation and a pronounced stretching of the bacterial cell envelope as the pressure escalates from 5 MPa (300 mOsm) to 125.30 MPa (0 mOsm). The graphical representation, particularly the conspicuous red regions on the graphs, vividly illustrates the significant alterations and stretching experienced by the bacteria under these varied pressure conditions. This aligns with the expected mechanical responses of Gram-positive bacteria and underscores the model's capacity to predict and elucidate the intricate deformations inherent in the thin shell structure under different pressure regimes.

Our exploration extended to predicting the mechanical responses exhibited by Gram-positive bacteria under varying pressure conditions, as elucidated through the material displacement contour in Figure 4.6. The interplay between pressure and mechanical behavior is vividly portrayed, where escalating pressure levels correspond to heightened tension within the Gram-positive bacterial structure. This heightened tension, as graphically depicted by the conspicuous red regions in the figure, underscores the notable increase in deformation experienced by the bacteria.

The material displacement contour further reveals intriguing insights into the vulnerability of certain regions of the Gram-positive bacteria to rupture under elevated pressure scenarios. Specifically, regions characterized by concentrated stress and heightened strain become susceptible to rupture when subjected to higher pressures. Notably, the maximum displacement occurs in regions of the cell where mobility along the vertical z-axis is prevalent, emphasizing the localized nature of the mechanical responses exhibited by Gram-positive bacteria under the influence of varying pressure gradients.

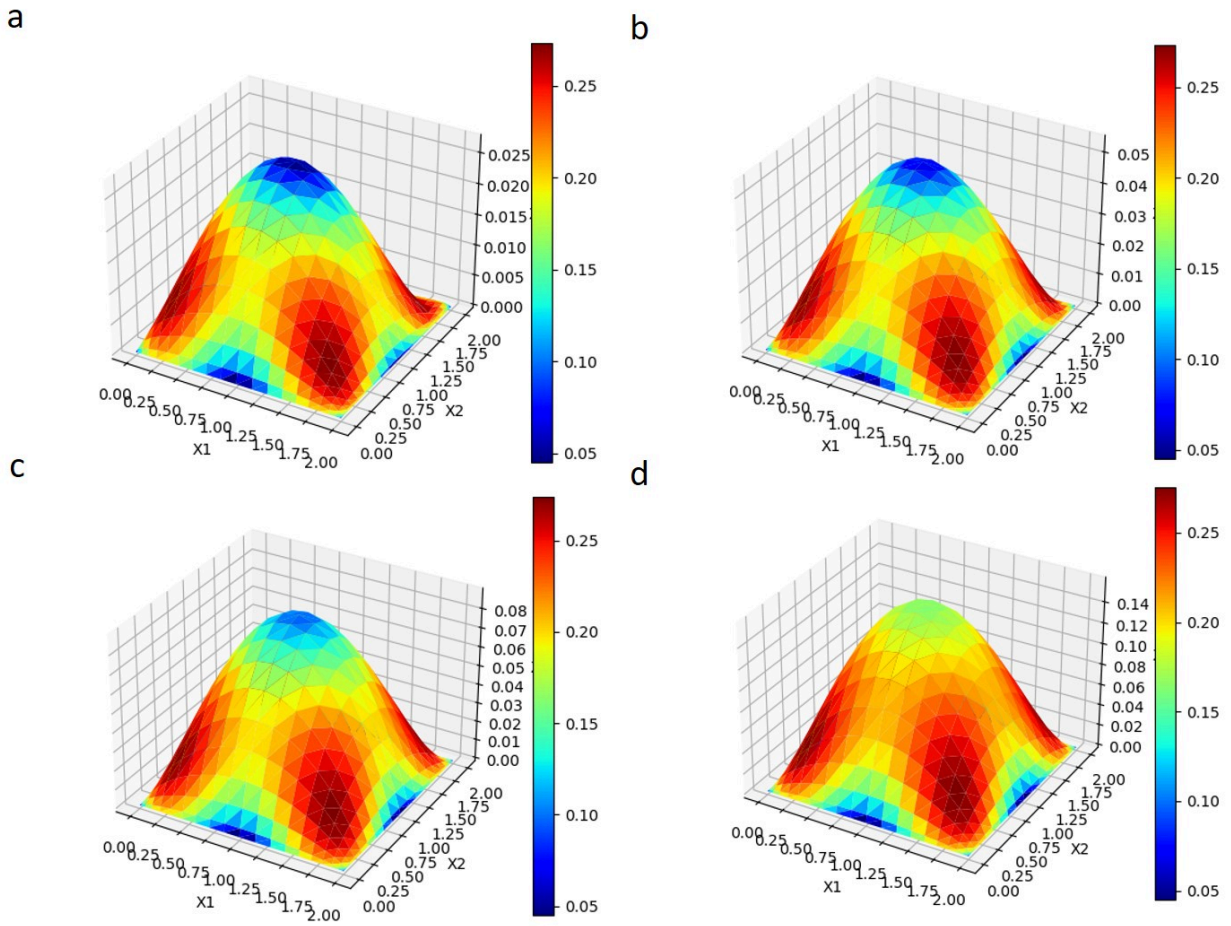

Figure 4.6: Material displacement contour a) $P_{lat} = 5$, b)$P_{lat} = 30.31$, c) $P_{lat} = 62.16$ and d)$P_{lat} = 125.30$ MPa which is normalized by the surface configuration.

As the bacteria membrane is considered a smooth surface in the X1 and X2 directions in our model, we assumed that the elevation of this surface in the X3 direction as the out-of-plane deformation, is comparable to the normalized radius values of bacteria under varying hypoosmotic pressures. Through this comparison, we essentially address how changes in membrane elevation representing a structural adaptation are aligned with changes in the measured size of the bacteria. A correlation between the predicted elevation and the experimental radius values is effective in capturing whether membrane mechanical response to hypoosmotic pressure is in agreement in terms of both experimental and theoretical viewpoints. Using our theoretical model, we calculated the dimensionless maximum and average elevation values, and the results are depicted in Figure 4.7.

The comparison between the normalized radius of bacteria and the elevation reveals an increase in both parameters with rising lateral pressure or decreasing extracellular osmolarity. The maximum bacteria normalized radius of 0.20 occurs at the lowest extracellular osmolarity of 0 mOsm, whereas the minimum normalized radius of 0.09 is observed at the highest extracellular osmolarity. Additionally, the theoretical model predicts a maximum elevation of 0.41 at this osmolarity.

For a more precise comparison with experimental results, we juxtaposed the bacteria normalized radius values with the average elevation in the X3 direction. The figure illustrates an increase in the average elevation as osmolarity decreases to 0 mOsm. In terms of the average elevation, the predicted maximum value is 0.16, while the minimum is 0.02. Comparing the theoretical values of the elevation with the normalized values of the radius indicates a closer proximity between the predicted average elevation values and the experimental radius values.

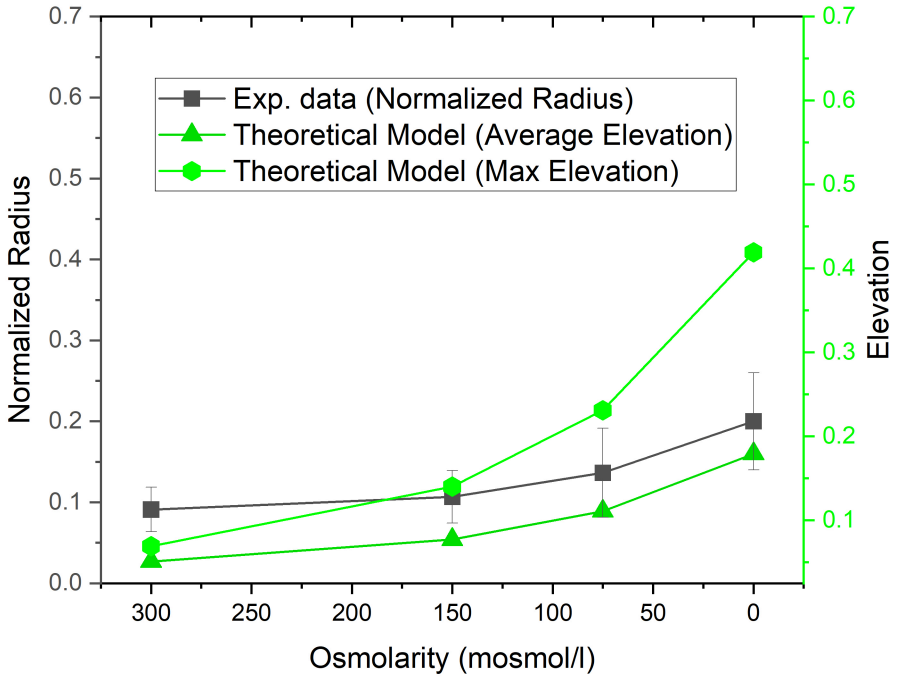

Figure 4.7: A comparison of the normalized Radius from experimental results with predicted maximum and average elevation from the theoretical model.

In this research work, we used the DLS technique to capture bacteria movements through measuring the frequency of the light when it scatters by bacteria motions in a suspension. This technique shines a laser towards the bacteria and captures how intensity of the scattered light fluctuates in a certain duration [127], [128].

By employing DLS, it is feasible to determine the diffusion coefficient of scattering particles. This coefficient establishes a relationship between diffusion and particle size through the Stokes–Einstein relationship [127]–[129].

$$D = \frac{K_B T}{6\pi\eta R} \tag{4.1}$$

where K_B is the Boltzmann constant, T is the temperature and η is the liquid viscosity and R is the particle radius [127]–[131].

As per the given equation, there exists a reciprocal relationship between diffusion and the hydrodynamic radius of the particle when illuminated by light [128]–[131]. Hence, with an increase in the radius of bacteria in our study, the diffusion of light in particles might be observed to decrease [132]. Consequently, the bacteria suspension exposed to 0 mOsm hypoosmotic pressure in our research may exhibit lower light diffusion compared to other samples. In the same direction, other studies have highlighted a correlation between the scattering of particles and their hydrodynamic sizes, as illustrated in the following equation [133]–[135].

$$C_{sca} = \pi r^2 Q_{sca}(\frac{r}{\lambda_m}, \frac{n_s}{n_m}) \tag{4.2}$$

In the provided equation, r represents the hydrodynamic radius of the particle, Q_{sca} is defined as scattering efficiency of the particle, λ_m stands for the wavelength of the light in

the medium, n_s denotes refractive index of the particle, and n_m is the refractive index of the medium [135]. Hence, there exists a direct correlation between the hydrodynamic radius of bacteria and the extent of light scattered by the bacteria [133]. This implies that larger bacteria colonies exhibit a more pronounced ability to scatter light.

When light interacts with a particle, it can either scatter within the particle or, if not diffused into the particle, scatter into the surrounding medium. Therefore, the bacterial sample with the highest radius is expected to exhibit increased light scattering and reduced diffusion.

It is also reported that the level of light scattering can be associated with the shape of the particle. In this hypothesis, the particle is regarded as a cylinder, and the shape of the particle is defined by the ratio of radius to length [133]. It indicates that as the radius increases and the length decreases, the shape of the particle can experience a transition from a cylinder to a sphere [136]. During this transition from a non-spherical to a semi-spherical shape due to applied hypoosmotic pressure, the particle's light scattering is anticipated to increase. This expectation aligns with the DLS results, indicating an increased radius of bacteria under hypoosmotic pressure exposure, suggesting morphological changes from non-spherical to semi-spherical shapes, resulting in higher light scattering. To further investigate these morphological changes, Transmission Electron Microscopy (TEM) was conducted.

The introduction of water into bacterial cells under hypoosmotic conditions induces cellular swelling, a phenomenon contingent upon the extent of hypoosmolarity. In instances of a rapid and excessive influx of water, the cellular envelope may undergo a critical point, culminating in osmotic lysis—the rupture of the cell membrane—and subsequent release of intracellular contents into the extracellular milieu [137], [138]. Furthermore, the dynamic influence of water influx extends beyond cellular integrity to encompass morphological alterations [137]. Particularly in the context of Gram-positive bacteria, the structural transition

from a rod-shaped configuration to a rounded or distorted morphology is observed as a consequence of hypoosmotic exposure [136].

The comprehensive examination of TEM images in Figure 4.8. pertaining to *L. acidophilus* reveals a discernible reduction in bacterial length concomitant with a transformative shift towards an round morphology. This morphological transition becomes particularly evident upon subjecting the bacterial culture to a marked reduction in osmolarity, specifically from an initial level of 300 mOsM to a diminished state of 0 mOsM. The observed alterations in bacterial dimensions and shape under varying osmotic conditions accentuate the pronounced sensitivity of Gram-positive bacteria to changes in their extracellular environment. Assuming a cylindrical shape for bacteria under the initial hypoosmotic pressure condition (Figure 4.8a), there is a noticeable increase in the radius/length ratio, indicating bacterial swelling with decreasing osmolarity. This observation from TEM analysis aligns with the hypothesis suggesting a correlation between the enhanced light scattering and the hydrodynamic radius results obtained from DLS tests and the shape change of bacteria.

The TEM images of the shape change of bacteria indicate a substantial transformation in regions where the membrane was initially almost flat, and experienced noticeable curvature with decreasing osmolarity. These observations affirm that the bacteria membrane undergoes both extension and localized bending in response to changes in osmolarity.

This analytical insight not only provides valuable information about the adaptability of Gram-positive to osmotic fluctuations but also contributes to the broader understanding of microbial responses to environmental stimuli, underscores the agreement between theoretical predictions and experimental observations.

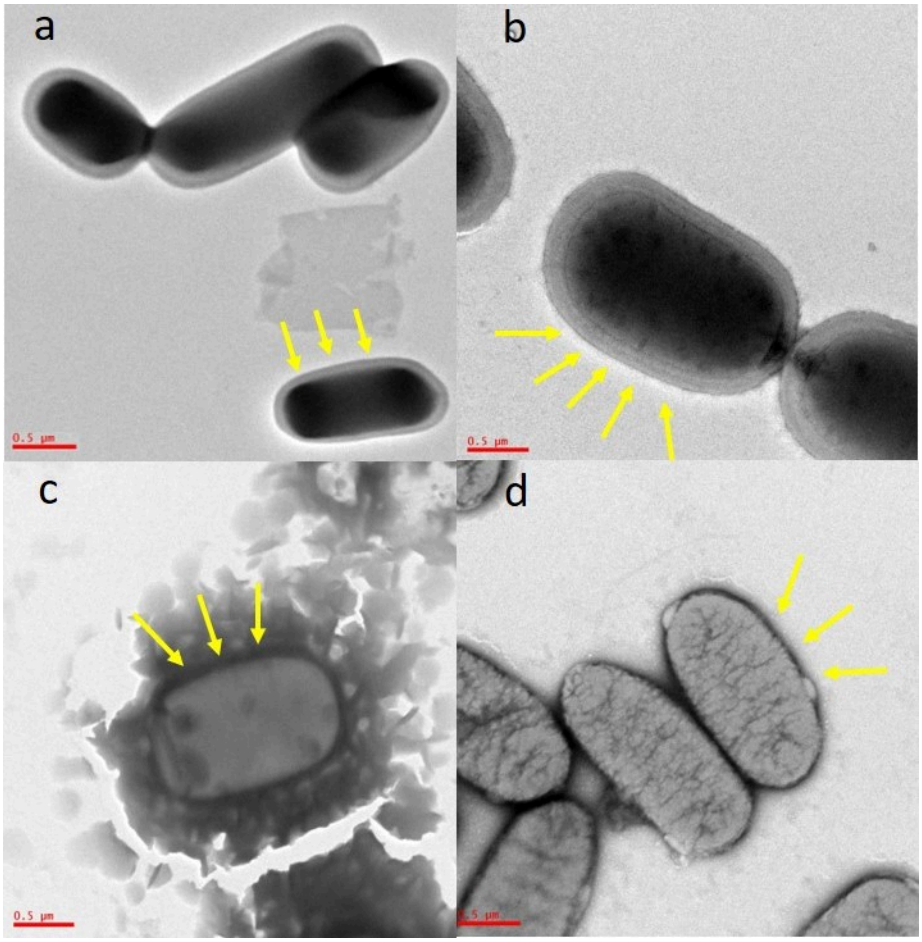

Figure 4.8: TEM micrographs of morphological changes of *L. acidophilus* when exposed to various hypoosmotic pressures of a) 300 mosmol/l, b) 150 mosmol/l, c) 75 mosmol/l and d) 0 mosmol/l.

4.3 Challenges and Opportunities in Bacteria Mechanical Response Study

While the findings of this thesis contribute valuable insights to the understanding of bacteria mechanical responses to the hypoosmotic pressure, it is important to acknowledge certain limitations in the obtained results. These limitations, inherent to the research design and methodologies employed, provide context for the interpretation of results and offer opportunities for future research refinement.

While we meticulously controlled certain variables, such as maintaining a consistent temperature and pH throughout the experiment and analysis, the methodologies employed for characterizing bacteria response to hypoosmotic pressure inherently carry limitations. Dynamic Light Scattering (DLS), employed for its reliability in capturing changes in bacterial size, has its constraints. Specifically, when the size of bacteria surpasses a certain threshold, DLS may inaccurately measure size changes. Consequently, the results obtained may not be representative of the entire cultured bacteria population.

Furthermore, the method assumes monodispersity; if there is considerable polydispersity among bacterial colonies, it could lead to a broader size distribution with a higher standard deviation. These factors may influence the precision and applicability of the results, although the main limitation of this method is that it does not provide any information about the shape change or morphological alternations of bacteria.

Our model offers predictions regarding shape changes in terms of curvature. However, the data obtained from the Dynamic Light Scattering (DLS) test only pertains to changes in size and the relationship between the hydrodynamic size of bacteria and their diffusion and light scattering. Besides, The challenge in this investigation lies in whether the discerned alteration in shape, transitioning from a non-spherical to semi-spherical configuration, is

exclusively associated with light scattering and the imposed DLS conditions. Alternatively, one must consider the potential influence of other parameters, including the nuances of bacteria culturing, on the observed morphological transformation.

In terms of Transmission Electron Microscopy (TEM) analysis, several limitations affect the study of bacteria morphological changes. The process involves specific preparation steps like fixation and staining, potentially introducing alterations to the original morphology. Additionally, TEM provides a 2D projection of a 3D shape, leading to potential misinterpretation of the actual structural arrangement and measurements of shape alterations.

Drawbacks include the cost, the need for specialized equipment, and the requirement for expertise. While TEM was employed to observe morphological changes like bacterial swelling under hypoosmotic pressure, accurately capturing information about the curvature of bacteria proves challenging due to these limitations. In summary, experimental results obtained from a dynamic suspension of bacteria may face constraints, impacting the correlation between experimental analysis and prediction models.

Despite the outlined limitations in the methodologies of this research, several future possibilities exist to enhance the study of bacteria mechanical responses to hypoosmotic pressure, including morphological information.

- One potential solution involves the adoption of modern imaging techniques capable of overcoming the limitations associated with 3D projection, allowing for the accurate capture of morphological curvature values at a potentially reduced cost.

- Another avenue for improvement is the exploration of hybrid approaches, integrating information from various characterization techniques such as Dynamic Light Scattering (DLS), Transmission Electron Microscopy (TEM), and Atomic Force Microscopy (AFM).

- Innovative sample preparation methods could be devised to minimize experimental side effects. For instance, the adoption of new fixation and stain-free imaging techniques might help preserve the original morphological shape of bacteria samples.

- The utilization of advanced image analysis software presents an opportunity to quantitatively study structural changes in bacteria. Real-time imaging approaches, enabling the capture of structural changes over time, could also be explored.

- Implementing diverse analysis approaches, including the application of machine learning algorithms, holds promise for predicting additional bacteria parameters, such as hydrodynamic radius, and establishing their relation with morphological changes.

These future possibilities create the potential to overcome current limitations of bacterial behavior to hypoosmotic pressure and achieve more detailed and accurate analysis.

Chapter 5

Conclusion

Bacteria are categorized based on their structure into two groups: Gram-positive and Gram-negative. The difference in their cellular structure creates unique bacteria cell that responses differently when they are exposed to the environmental conditions such as osmotic pressure. In this work, we used experimental tools to study Gram-negative and Gram-positive bacteria responses to hypoosmotic pressure, followed by developing a mathematical model to predict the mechanical responses of Gram-positive bacteria.

We developed Helfrich model to gain partial development equations which emphasizes on responses of membrane-peptidoglycan assembly in bacteria. The Newton-Raphson method served as the computational tool for solving the equations and was incorporated into the FENICS platform, an open-source Python-based solver. The important results are presented as follow.

- Decreased extracellular osmolarity provides much swelling and extension in both bacteria types which leads to increased radius of bacteria through DLS test analysis.

- The highest radius quantity is obtained by adding DI water (mOsm) to *L. acidophilus*

bacteria cells which is almost 1.79±0.06 μm.

- By decreasing extracellular osmolarity from 300 mOsm to 0 mOsm, *L. acidophilus* radius increases from 0.81±0.05 μm to 1.79±0.12 μm, although *E. coli* witnesses radius change from 0.45±0.008 μm to 0.67±0.018 μm.

- In addition, the difference between external and internal pressure (Turgor pressure) increases, resulting in remarkably increased lateral pressure which is applied on the inner membrane and peptidoglycan layers in bacteria. This leads to expansion and also providing mechanical force on bacteria.

- Morphological changes of Gram-positive bacteria was captured using TEM analysis which showed shape changes by decreasing osmolarity. The results from experimental and theoretical analysis were compared and represented well agreement, which shows that the proposed model is able to predict bacteria responses based on specific material property.

- Simulated deformation contours are sensitive to material properties such as pressure. By increasing the applied pressure to 125.30 MPa, deformed area under stress is extended significantly.

- Using the Finite Element method, the iterative solver in our proposed model indicated that the solution is converging in each iteration through reduction in residual quantities.

- Gram-positive bacteria are predicted to undergo substantial out-of-plane deformation along the z-direction as lateral pressure increases from 5 MPa to 125.30 MPa. This deformation is visually represented by the red regions on the deformation contours of the model, vividly illustrating the stretching of bacteria under diverse pressure conditions.

- The increased tension experienced by the bacteria under various pressure conditions is visually depicted on the Material Displacement Contour. This representation offers valuable insights into the susceptibility of certain regions within Gram-positive bacteria to rupture when subjected to elevated pressure. Specifically, areas characterized by concentrated stress and heightened strain are prone to rupture under increased pressures. It is noteworthy that the maximum displacement occurs in regions of the cell where mobility along the vertical z-axis is prevalent.

To sum up, we addressed a comparison between Gram-negative and Gram-positive size change using experimental tools and applying different pressure conditions. Besides, we successfully predicted Gram-positive mechanical responses under hypoosmotic pressure by employing PDE systems to investigate the deformation contours in several conditions.

The investigation of morphological changes induced by osmotic pressure, along with the creation of an associated mathematical model, offers substantial potential in the realm of biomedical applications. These applications encompass the refinement and optimization of therapeutic approaches for drug delivery and various tissue-related treatments.

It is interesting to note that there are always some limitations in prediction of bacteria responses since they possess a kind of complex structure with many unknown characteristics, although they have been investigated over the past decades. It is recommended that theoretical study of bacteria needs to be investigated by considering the role of each subcomponent such as proteins in cell wall layers when bacteria is exposed to environmental pressure.

References

[1] E. Zuckerkandl and L. Pauling, "Molecules as documents of evolutionary history," *Journal of theoretical biology*, vol. 8, no. 2, pp. 357–366, 1965.

[2] E. F. DeLong and N. R. Pace, "Environmental diversity of bacteria and archaea," *Systematic biology*, vol. 50, no. 4, pp. 470–478, 2001.

[3] C. R. Woese and G. E. Fox, "Phylogenetic structure of the prokaryotic domain: The primary kingdoms," *Proceedings of the National Academy of Sciences*, vol. 74, no. 11, pp. 5088–5090, 1977.

[4] D. A. Stahl, D. J. Lane, G. J. Olsen, and N. R. Pace, "Analysis of hydrothermal vent-associated symbionts by ribosomal rna sequences," *Science*, vol. 224, no. 4647, pp. 409–411, 1984.

[5] N. R. Pace, D. A. Stahl, D. J. Lane, and G. J. Olsen, "The analysis of natural microbial populations by ribosomal rna sequences," *Advances in microbial ecology*, pp. 1–55, 1986.

[6] R. Karlsson, L. Gonzales-Siles, F. Boulund, *et al.*, "Proteotyping: Proteomic characterization, classification and identification of microorganisms–a prospectus," *Systematic and applied microbiology*, vol. 38, no. 4, pp. 246–257, 2015.

[7] G. K. Auer and D. B. Weibel, "Bacterial cell mechanics," *Biochemistry*, vol. 56, no. 29, pp. 3710–3724, 2017.

[8] V. Vadillo-Rodríguez and J. R. Dutcher, "Viscoelasticity of the bacterial cell envelope," *Soft Matter*, vol. 7, no. 9, pp. 4101–4110, 2011.

[9] R. Buda, Y. Liu, J. Yang, *et al.*, "Dynamics of escherichia coli's passive response to a sudden decrease in external osmolarity," *Proceedings of the National Academy of Sciences*, vol. 113, no. 40, E5838–E5846, 2016.

[10] E. L. Fiscus, "The interaction between osmotic-and pressure-induced water flow in plant roots," *Plant Physiology*, vol. 55, no. 5, pp. 917–922, 1975.

[11] M. Mathelié-Guinlet, A. T. Asmar, J.-F. Collet, and Y. F. Dufrêne, "Bacterial cell mechanics beyond peptidoglycan," *Trends in microbiology*, vol. 28, no. 9, pp. 706–708, 2020.

[12] S. Jordan, M. I. Hutchings, and T. Mascher, "Cell envelope stress response in gram-positive bacteria," *FEMS microbiology reviews*, vol. 32, no. 1, pp. 107–146, 2008.

[13] G.-W. Li, D. Burkhardt, C. Gross, and J. S. Weissman, "Quantifying absolute protein synthesis rates reveals principles underlying allocation of cellular resources," *Cell*, vol. 157, no. 3, pp. 624–635, 2014.

[14] G. D. Shockman and J. F. Barren, "Structure, function, and assembly of cell walls of gram-positive bacteria," *Annual review of microbiology*, vol. 37, no. 1, pp. 501–527, 1983.

[15] J. Sun, S. T. Rutherford, T. J. Silhavy, and K. C. Huang, "Physical properties of the bacterial outer membrane," *Nature Reviews Microbiology*, vol. 20, no. 4, pp. 236–248, 2022.

[16] S. Garde, P. K. Chodisetti, and M. Reddy, "Peptidoglycan: Structure, synthesis, and regulation," *EcoSal Plus*, vol. 9, no. 2, 2021.

[17] W. Vollmer, "Structure and biosynthesis of the murein (peptidoglycan) sacculus," *The periplasm*, pp. 198–213, 2006.

[18] L. Gan, S. Chen, and G. J. Jensen, "Molecular organization of gram-negative peptidoglycan," *Proceedings of the National Academy of Sciences*, vol. 105, no. 48, pp. 18 953–18 957, 2008.

[19] M. Beeby, J. C. Gumbart, B. Roux, and G. J. Jensen, "Architecture and assembly of the g ram-positive cell wall," *Molecular microbiology*, vol. 88, no. 4, pp. 664–672, 2013.

[20] V. R. Matias and T. J. Beveridge, "Cryo-electron microscopy reveals native polymeric cell wall structure in bacillus subtilis 168 and the existence of a periplasmic space," *Molecular microbiology*, vol. 56, no. 1, pp. 240–251, 2005.

[21] W. Vollmer and S. J. Seligman, "Architecture of peptidoglycan: More data and more models," *Trends in microbiology*, vol. 18, no. 2, pp. 59–66, 2010.

[22] S. J. Kim, J. Chang, and M. Singh, "Peptidoglycan architecture of gram-positive bacteria by solid-state nmr," *Biochimica et Biophysica Acta (BBA)-Biomembranes*, vol. 1848, no. 1, pp. 350–362, 2015.

[23] V. R. Matias and T. J. Beveridge, "Native cell wall organization shown by cryo-electron microscopy confirms the existence of a periplasmic space in staphylococcus aureus," *Journal of bacteriology*, vol. 188, no. 3, pp. 1011–1021, 2006.

[24] P. Jafarei and M. T. Ebrahimi, "Lactobacillus acidophilus cell structure and application," *African Journal of Microbiology Research*, vol. 5, no. 24, pp. 4033–4042, 2011.

[25] J. M. Wood, "Osmosensing by bacteria," *Science's STKE*, vol. 2006, no. 357, pe43–pe43, 2006.

[26] E. Bremer and R. Krämer, "Responses of microorganisms to osmotic stress," *Annual review of Microbiology*, vol. 73, pp. 313–334, 2019.

[27] R. Krämer, "Bacterial stimulus perception and signal transduction: Response to osmotic stress," *The Chemical Record*, vol. 10, no. 4, pp. 217–229, 2010.

[28] J. M. Wood, "Osmosensing by bacteria: Signals and membrane-based sensors," *Microbiology and molecular biology reviews*, vol. 63, no. 1, pp. 230–262, 1999.

[29] A. J. Egan, J. Errington, and W. Vollmer, "Regulation of peptidoglycan synthesis and remodelling," *Nature Reviews Microbiology*, vol. 18, no. 8, pp. 446–460, 2020.

[30] J. v. Heijenoort, "Formation of the glycan chains in the synthesis of bacterial peptidoglycan," *Glycobiology*, vol. 11, no. 3, 25R–36R, 2001.

[31] A. Typas, M. Banzhaf, C. A. Gross, and W. Vollmer, "From the regulation of peptidoglycan synthesis to bacterial growth and morphology," *Nature Reviews Microbiology*, vol. 10, no. 2, pp. 123–136, 2012.

[32] B. Dmitriev, F. Toukach, and S. Ehlers, "Towards a comprehensive view of the bacterial cell wall," *Trends in microbiology*, vol. 13, no. 12, pp. 569–574, 2005.

[33] B. Corry and B. Martinac, "Bacterial mechanosensitive channels: Experiment and theory," *Biochimica et Biophysica Acta (BBA)-Biomembranes*, vol. 1778, no. 9, pp. 1859–1870, 2008.

[34] M. D. Edwards, S. Black, T. Rasmussen, *et al.*, "Characterization of three novel mechanosensitive channel activities in escherichia coli," *Channels*, vol. 6, no. 4, pp. 272–281, 2012.

[35] B. Martinac, M. Buechner, A. H. Delcour, J. Adler, and C. Kung, "Pressure-sensitive ion channel in escherichia coli.," *Proceedings of the National Academy of Sciences*, vol. 84, no. 8, pp. 2297–2301, 1987.

[36] P. Blount and I. Iscla, "Life with bacterial mechanosensitive channels, from discovery to physiology to pharmacological target," *Microbiology and Molecular Biology Reviews*, vol. 84, no. 1, pp. 10–1128, 2020.

[37] P. Blount, S. I. Sukharev, P. C. Moe, B. Martinac, and C. Kung, "[24] mechanosensitive channels of bacteria," *Methods in enzymology*, vol. 294, pp. 458–482, 1999.

[38] H.-J. Ruthe and J. Adler, "Fusion of bacterial spheroplasts by electric fields," *Biochimica et Biophysica Acta (BBA)-Biomembranes*, vol. 819, no. 1, pp. 105–113, 1985.

[39] B. Martinac, J. Adler, and C. Kung, "Mechanosensitive ion channels of e. coli activated by amphipaths," *Nature*, vol. 348, no. 6298, pp. 261–263, 1990.

[40] C. BERRIER, A. COULOMBE, I. SZABO, M. ZORATTI, and A. GHAZI, "Gadolinium ion inhibits loss of metabolites induced by osmotic shock and large stretch-activated channels in bacteria," *European Journal of Biochemistry*, vol. 206, no. 2, pp. 559–565, 1992.

[41] I. Szabó, V. Petronilli, and M. Zoratti, "A patch-clamp investigation of the streptococcus faecalis cell membrane," *The Journal of membrane biology*, vol. 131, pp. 203–218, 1993.

[42] M. Boer, A. Anishkin, and S. Sukharev, "Adaptive mscs gating in the osmotic permeability response in e. coli: The question of time," *Biochemistry*, vol. 50, no. 19, pp. 4087–4096, 2011.

[43] C. Kung, B. Martinac, and S. Sukharev, "Mechanosensitive channels in microbes," *Annual review of microbiology*, vol. 64, pp. 313–329, 2010.

[44] S. L. Grage, A. M. Keleshian, T. Turdzeladze, *et al.*, "Bilayer-mediated clustering and functional interaction of mscl channels," *Biophysical journal*, vol. 100, no. 5, pp. 1252–1260, 2011.

[45] P. MITCHELL, "Osmotic function and struture in bacteria," in *Symp. Soc. Gen. Microbiol.*, vol. 6, 1956, pp. 150–180.

[46] Y. Deng, M. Sun, and J. W. Shaevitz, "Direct measurement of cell wall stress stiffening and turgor pressure in live bacterial cells," *Physical review letters*, vol. 107, no. 15, p. 158 101, 2011.

[47] I. R. Booth, "Bacterial mechanosensitive channels: Progress towards an understanding of their roles in cell physiology," *Current Opinion in Microbiology*, vol. 18, pp. 16–22, 2014.

[48] P. Blount, M. J. Schroeder, and C. Kung, "Mutations in a bacterial mechanosensitive channel change the cellular response to osmotic stress," *Journal of Biological Chemistry*, vol. 272, no. 51, pp. 32 150–32 157, 1997.

[49] I. R. Booth, S. Miller, A. Müller, and L. Lehtovirta-Morley, "The evolution of bacterial mechanosensitive channels," *Cell Calcium*, vol. 57, no. 3, pp. 140–150, 2015.

[50] Y. Nakamaru, Y. Takahashi, T. Unemoto, and T. Nakamura, "Mechanosensitive channel functions to alleviate the cell lysis of marine bacterium, vibrio alginolyticus, by osmotic downshock," *FEBS letters*, vol. 444, no. 2-3, pp. 170–172, 1999.

[51] N. Levina, S. Tötemeyer, N. R. Stokes, P. Louis, M. A. Jones, and I. R. Booth, "Protection of escherichia coli cells against extreme turgor by activation of mscs and mscl mechanosensitive channels: Identification of genes required for mscs activity," *The EMBO journal*, vol. 18, no. 7, pp. 1730–1737, 1999.

[52] I. R. Booth and P. Blount, "The mscs and mscl families of mechanosensitive channels act as microbial emergency release valves," *Journal of bacteriology*, vol. 194, no. 18, pp. 4802–4809, 2012.

[53] S. Sukharev, M. Betanzos, C.-S. Chiang, and H. R. Guy, "The gating mechanism of the large mechanosensitive channel mscl," *Nature*, vol. 409, no. 6821, pp. 720–724, 2001.

[54] E. Evans and D. Needham, "Physical properties of surfactant bilayer membranes: Thermal transitions, elasticity, rigidity, cohesion and colloidal interactions," *Journal of Physical Chemistry*, vol. 91, no. 16, pp. 4219–4228, 1987.

[55] C. Kapsalis, B. Wang, H. El Mkami, *et al.*, "Allosteric activation of an ion channel triggered by modification of mechanosensitive nano-pockets," *Nature Communications*, vol. 10, no. 1, p. 4619, 2019.

[56] Y. Wang, Y. Liu, H. A. DeBerg, *et al.*, "Single molecule fret reveals pore size and opening mechanism of a mechano-sensitive ion channel," *Elife*, vol. 3, e01834, 2014.

[57] E. Perozo, D. M. Cortes, P. Sompornpisut, A. Kloda, and B. Martinac, "Open channel structure of mscl and the gating mechanism of mechanosensitive channels," *Nature*, vol. 418, no. 6901, pp. 942–948, 2002.

[58] R. B. Bass, P. Strop, M. Barclay, and D. C. Rees, "Crystal structure of escherichia coli mscs, a voltage-modulated and mechanosensitive channel," *Science*, vol. 298, no. 5598, pp. 1582–1587, 2002.

[59] J. H. Naismith and I. R. Booth, "Bacterial mechanosensitive channels—mscs: Evolution's solution to creating sensitivity in function," *Annual review of biophysics*, vol. 41, pp. 157–177, 2012.

[60] J. Gullingsrud and K. Schulten, "Lipid bilayer pressure profiles and mechanosensitive channel gating," *Biophysical journal*, vol. 86, no. 6, pp. 3496–3509, 2004.

[61] A. Lee, "Lipid–protein interactions in biological membranes: A structural perspective," *Biochimica et Biophysica Acta (BBA)-Biomembranes*, vol. 1612, no. 1, pp. 1–40, 2003.

[62] S. H. White, A. S. Ladokhin, S. Jayasinghe, and K. Hristova, "How membranes shape protein structure," *Journal of Biological Chemistry*, vol. 276, no. 35, pp. 32 395–32 398, 2001.

[63] J. A. Killian and G. von Heijne, "How proteins adapt to a membrane–water interface," *Trends in biochemical sciences*, vol. 25, no. 9, pp. 429–434, 2000.

[64] A. Rasmussen, T. Rasmussen, M. D. Edwards, *et al.*, "The role of tryptophan residues in the function and stability of the mechanosensitive channel mscs from escherichia coli," *Biochemistry*, vol. 46, no. 38, pp. 10 899–10 908, 2007.

[65] T. Nomura, M. Sokabe, and K. Yoshimura, "Lipid-protein interaction of the mscs mechanosensitive channel examined by scanning mutagenesis," *Biophysical journal*, vol. 91, no. 8, pp. 2874–2881, 2006.

[66] K. Okada, P. C. Moe, and P. Blount, "Functional design of bacterial mechanosensitive channels: Comparisons and contrasts illuminated by random mutagenesis," *Journal of Biological Chemistry*, vol. 277, no. 31, pp. 27 682–27 688, 2002.

[67] G. Calamita, *Advances in aquaporins*, 2023.

[68] K. Murata, K. Mitsuoka, T. Hirai, *et al.*, "Structural determinants of water permeation through aquaporin-1," *Nature*, vol. 407, no. 6804, pp. 599–605, 2000.

[69] A. Froger, J.-P. Rolland, P. Bron, *et al.*, "Functional characterization of a microbial aquaglyceroporin," *Microbiology*, vol. 147, no. 5, pp. 1129–1135, 2001.

[70] G. Benga, "Water channel proteins (later called aquaporins) and relatives: Past, present, and future," *IUBMB life*, vol. 61, no. 2, pp. 112–133, 2009.

[71] G. Ren, A. Cheng, V. Reddy, P. Melnyk, and A. K. Mitra, "Three-dimensional fold of the human aqp1 water channel determined at 4 Å resolution by electron crystal-

lography of two-dimensional crystals embedded in ice," *Journal of molecular biology*, vol. 301, no. 2, pp. 369–387, 2000.

[72] C. Li and W. Wang, "Molecular biology of aquaporins," *Aquaporins*, pp. 1–34, 2017.

[73] K. Takata, T. Matsuzaki, and Y. Tajika, "Aquaporins: Water channel proteins of the cell membrane," *Progress in histochemistry and cytochemistry*, vol. 39, no. 1, pp. 1–83, 2004.

[74] K. Ishibashi, S. Kondo, S. Hara, and Y. Morishita, "The evolutionary aspects of aquaporin family," *American Journal of Physiology-Regulatory, Integrative and Comparative Physiology*, vol. 300, no. 3, R566–R576, 2011.

[75] K. Hedfalk, R. M. Bill, J. G. Mullins, *et al.*, "A regulatory domain in the c-terminal extension of the yeast glycerol channel fps1p," *Journal of Biological Chemistry*, vol. 279, no. 15, pp. 14 954–14 960, 2004.

[76] A. Engel, Y. Fujiyoshi, T. Gonen, and T. Walz, "Junction-forming aquaporins," *Current opinion in structural biology*, vol. 18, no. 2, pp. 229–235, 2008.

[77] H. Viadiu, T. Gonen, and T. Walz, "Projection map of aquaporin-9 at 7 Å resolution," *Journal of molecular biology*, vol. 367, no. 1, pp. 80–88, 2007.

[78] J. S. Hub and B. L. De Groot, "Mechanism of selectivity in aquaporins and aquaglyceroporins," *Proceedings of the National Academy of Sciences*, vol. 105, no. 4, pp. 1198–1203, 2008.

[79] G. Fischer, U. Kosinska-Eriksson, C. Aponte-Santamaría, *et al.*, "Crystal structure of a yeast aquaporin at 1.15 Å reveals a novel gating mechanism," *PLoS biology*, vol. 7, no. 6, e1000130, 2009.

[80] H. Zhang and A. Verkman, "Evidence against involvement of aquaporin-4 in cell–cell adhesion," *Journal of molecular biology*, vol. 382, no. 5, pp. 1136–1143, 2008.

[81] T. Gonen and T. Walz, "The structure of aquaporins," *Quarterly reviews of biophysics*, vol. 39, no. 4, pp. 361–396, 2006.

[82] H. Tong, Q. Hu, L. Zhu, and X. Dong, "Prokaryotic aquaporins," *Cells*, vol. 8, no. 11, p. 1316, 2019.

[83] D. F. Savage, P. F. Egea, Y. Robles-Colmenares, J. D. O. III, and R. M. Stroud, "Architecture and selectivity in aquaporins: 2.5 Å x-ray structure of aquaporin z," *PLoS biology*, vol. 1, no. 3, e72, 2003.

[84] D. Fu, A. Libson, L. J. Miercke, *et al.*, "Structure of a glycerol-conducting channel and the basis for its selectivity," *science*, vol. 290, no. 5491, pp. 481–486, 2000.

[85] P. Agre, M. J. Borgnia, M. Yasui, *et al.*, "Discovery of the aquaporins and their impact on basic and clinical physiology," 2001.

[86] F. Zhu, E. Tajkhorshid, and K. Schulten, "Theory and simulation of water permeation in aquaporin-1," *Biophysical journal*, vol. 86, no. 1, pp. 50–57, 2004.

[87] A. Finkelstein, "Water movement through lipid bilayers, pores, and plasma membranes.," *(No Title)*, 1987.

[88] A. L. Koch, M. L. Higgins, and R. J. Doyle, "The role of surface stress in the morphology of microbes," *Microbiology*, vol. 128, no. 5, pp. 927–945, 1982.

[89] C. E. Harper and C. J. Hernandez, "Cell biomechanics and mechanobiology in bacteria: Challenges and opportunities," *APL bioengineering*, vol. 4, no. 2, 2020.

[90] M. Deserno, "Fluid lipid membranes: From differential geometry to curvature stresses," *Chemistry and physics of lipids*, vol. 185, pp. 11–45, 2015.

[91] P. Bassereau, B. Sorre, and A. Lévy, "Bending lipid membranes: Experiments after w. helfrich's model," *Advances in colloid and interface science*, vol. 208, pp. 47–57, 2014.

[92] E. Evans, A. Yeung, R. Waugh, and J. Song, "Dynamic coupling and nonlocal curvature elasticity in bilayer membranes," in *The Structure and Conformation of Amphiphilic Membranes: Proceedings of the International Workshop on Amphiphilic Membranes, Jülich, Germany, September 16–18, 1991*, Springer, 1992, pp. 148–153.

[93] U. Seifert, "Configurations of fluid membranes and vesicles," *Advances in physics*, vol. 46, no. 1, pp. 13–137, 1997.

[94] F. Campelo, C. Arnarez, S. J. Marrink, and M. M. Kozlov, "Helfrich model of membrane bending: From gibbs theory of liquid interfaces to membranes as thick anisotropic elastic layers," *Advances in colloid and interface science*, vol. 208, pp. 25–33, 2014.

[95] J. W. Gibbs, "On the equilibrium of heterogeneous substances," *American journal of science*, vol. 3, no. 96, pp. 441–458, 1878.

[96] M. P. Do Carmo, *Differential geometry of curves and surfaces: revised and updated second edition*. Courier Dover Publications, 2016.

[97] W. Helfrich, "Elastic properties of lipid bilayers: Theory and possible experiments," *Zeitschrift für Naturforschung c*, vol. 28, no. 11-12, pp. 693–703, 1973.

[98] E. Gladilin, A. Micoulet, B. Hosseini, K. Rohr, J. Spatz, and R. Eils, "3d finite element analysis of uniaxial cell stretching: From image to insight," *Physical biology*, vol. 4, no. 2, p. 104, 2007.

[99] Y. Tang, G. Cao, X. Chen, J. Yoo, A. Yethiraj, and Q. Cui, "A finite element framework for studying the mechanical response of macromolecules: Application to the gating of the mechanosensitive channel mscl," *Biophysical journal*, vol. 91, no. 4, pp. 1248–1263, 2006.

[100] M. Kleerebezem, P. Hols, E. Bernard, *et al.*, "The extracellular biology of the lactobacilli," *FEMS microbiology reviews*, vol. 34, no. 2, pp. 199–230, 2010.

[101] A. Solimeno, R. Samsó, E. Uggetti, *et al.*, "New mechanistic model to simulate microalgae growth," *Algal Research*, vol. 12, pp. 350–358, 2015.

[102] H. Jiang, F. Si, W. Margolin, and S. X. Sun, "Mechanical control of bacterial cell shape," *Biophysical journal*, vol. 101, no. 2, pp. 327–335, 2011.

[103] A. Janshoff and C. Steinem, "Mechanics of lipid bilayers: What do we learn from pore-spanning membranes?" *Biochimica et Biophysica Acta (BBA)-Molecular Cell Research*, vol. 1853, no. 11, pp. 2977–2983, 2015.

[104] A. Boulbitch, B. Quinn, and D. Pink, "Elasticity of the rod-shaped gram-negative eubacteria," *Physical Review Letters*, vol. 85, no. 24, p. 5246, 2000.

[105] M. Islam, F. S. S. Aldawsari, and P. K. Yarlagadda, "Finite element modelling of a gram-negative bacterial cell and nanospike array for cell rupture mechanism study," *Molecules*, vol. 28, no. 5, p. 2184, 2023.

[106] H. Hwang, N. Paracini, J. M. Parks, J. H. Lakey, and J. C. Gumbart, "Distribution of mechanical stress in the escherichia coli cell envelope," *Biochimica et Biophysica Acta (BBA)-Biomembranes*, vol. 1860, no. 12, pp. 2566–2575, 2018.

[107] D. Jefferies, J. Shearer, and S. Khalid, "Role of o-antigen in response to mechanical stress of the e. coli outer membrane: Insights from coarse-grained md simulations," *The Journal of Physical Chemistry B*, vol. 123, no. 17, pp. 3567–3575, 2019.

[108] L. Zhao, T. Liu, X. Li, *et al.*, "Study of finite element simulation on the mechano-bactericidal mechanism of hierarchical nanostructure arrays," *ACS Biomaterials Science & Engineering*, vol. 9, no. 8, pp. 4770–4780, 2023.

[109] S. Ferdous, J. L. Dopp, and N. F. Reuel, "Optimization of e. coli tip-sonication for high-yield c ell-free extract using finite element modeling," *AIChE Journal*, vol. 67, no. 10, e17389, 2021.

[110] H. Wennerström and M. Oliveberg, "On the osmotic pressure of cells," *QRB Discovery*, vol. 3, e12, 2022.

[111] P. B. Canham, "The minimum energy of bending as a possible explanation of the biconcave shape of the human red blood cell," *Journal of theoretical biology*, vol. 26, no. 1, pp. 61–81, 1970.

[112] Z. Tu and Z. Ou-Yang, "Recent theoretical advances in elasticity of membranes following helfrich's spontaneous curvature model," *Advances in colloid and interface science*, vol. 208, pp. 66–75, 2014.

[113] F. C. Frank, "I. liquid crystals. on the theory of liquid crystals," *Discussions of the Faraday Society*, vol. 25, pp. 19–28, 1958.

[114] E. A. Evans, "Minimum energy analysis of membrane deformation applied to pipet aspiration and surface adhesion of red blood cells," *Biophysical journal*, vol. 30, no. 2, pp. 265–284, 1980.

[115] W. Helfrich and J. Prost, "Intrinsic bending force in anisotropic membranes made of chiral molecules," *Physical Review A*, vol. 38, no. 6, p. 3065, 1988.

[116] J. V. Selinger and J. M. Schnur, "Theory of chiral lipid tubules," *Physical review letters*, vol. 71, no. 24, p. 4091, 1993.

[117] P. Rangamani, A. Behzadan, and M. Holst, "Local sensitivity analysis of the "membrane shape equation" derived from the helfrich energy," *Mathematics and Mechanics of Solids*, vol. 26, no. 3, pp. 356–385, 2021.

[118] A. Agrawal and D. J. Steigmann, "Boundary-value problems in the theory of lipid membranes," *Continuum Mechanics and Thermodynamics*, vol. 21, pp. 57–82, 2009.

[119] D. Steigmann, E. Baesu, R. E. Rudd, J. Belak, and M. McElfresh, "On the variational theory of cell-membrane equilibria," *Interfaces and Free Boundaries*, vol. 5, no. 4, pp. 357–366, 2003.

[120] D. Marinkovic and M. Zehn, "Survey of finite element method-based real-time simulations," *Applied Sciences*, vol. 9, no. 14, p. 2775, 2019.

[121] H. Zahedmanesh and C. Lally, "A multiscale mechanobiological modelling framework using agent-based models and finite element analysis: Application to vascular tissue engineering," *Biomechanics and modeling in mechanobiology*, vol. 11, pp. 363–377, 2012.

[122] W. Zeng and G. Liu, "Smoothed finite element methods (s-fem): An overview and recent developments," *Archives of Computational Methods in Engineering*, vol. 25, no. 2, pp. 397–435, 2018.

[123] H. H. Tuson, G. K. Auer, L. D. Renner, *et al.*, "Measuring the stiffness of bacterial cells from growth rates in hydrogels of tunable elasticity," *Molecular microbiology*, vol. 84, no. 5, pp. 874–891, 2012.

[124] A. Amir, F. Babaeipour, D. B. McIntosh, D. R. Nelson, and S. Jun, "Bending forces plastically deform growing bacterial cell walls," *Proceedings of the National Academy of Sciences*, vol. 111, no. 16, pp. 5778–5783, 2014.

[125] G. Misra, E. R. Rojas, A. Gopinathan, and K. C. Huang, "Mechanical consequences of cell-wall turnover in the elongation of a gram-positive bacterium," *Biophysical journal*, vol. 104, no. 11, pp. 2342–2352, 2013.

[126] R. Han, X.-Q. Feng, W. Vollmer, P. Stoodley, and J. Chen, "Deciphering the adaption of bacterial cell wall mechanical integrity and turgor to different chemical or mechanical environments," *Journal of Colloid and Interface Science*, vol. 640, pp. 510–520, 2023.

[127] S. Vargas, B. E. Millán-Chiu, S. M. Arvizu-Medrano, A. M. Loske, and R. Rodríguez, "Dynamic light scattering: A fast and reliable method to analyze bacterial growth during the lag phase," *Journal of microbiological methods*, vol. 137, pp. 34–39, 2017.

[128] D. Germain, M. Leocmach, and T. Gibaud, "Differential dynamic microscopy to characterize brownian motion and bacteria motility," *American Journal of Physics*, vol. 84, no. 3, pp. 202–210, 2016.

[129] J. Stetefeld, S. A. McKenna, and T. R. Patel, "Dynamic light scattering: A practical guide and applications in biomedical sciences," *Biophysical reviews*, vol. 8, pp. 409–427, 2016.

[130] P. Arenas-Guerrero, Á. V. Delgado, K. J. Donovan, *et al.*, "Determination of the size distribution of non-spherical nanoparticles by electric birefringence-based methods," *Scientific Reports*, vol. 8, no. 1, p. 9502, 2018.

[131] A. A. S. Alzahrani, "Characterization of non-spherical nanoparticles using scattering techniques," Ph.D. dissertation, RMIT University, 2023.

[132] N. Ohtori, Y. Kondo, and Y. Ishii, "Molecular size and shape effects: Rotational diffusion and the stokes-einstein-debye relation," *Journal of Molecular Liquids*, vol. 314, p. 113 764, 2020.

[133] S. Johnsen and E. A. Widder, "The physical basis of transparency in biological tissue: Ultrastructure and the minimization of light scattering," *Journal of theoretical biology*, vol. 199, no. 2, pp. 181–198, 1999.

[134] H. van de Hulst, "Light scattering by small particles. new york (john wiley and sons), london (chapman and hall)," 1957.

[135] G. Mie, "Beiträge zur optik trüber medien, speziell kolloidaler metallösungen," *Annalen der physik*, vol. 330, no. 3, pp. 377–445, 1908.

[136] T. T. Cushnie, N. H. O'Driscoll, and A. J. Lamb, "Morphological and ultrastructural changes in bacterial cells as an indicator of antibacterial mechanism of action," *Cellular and molecular life sciences*, vol. 73, pp. 4471–4492, 2016.

[137] E. Rojas, J. A. Theriot, and K. C. Huang, "Response of escherichia coli growth rate to osmotic shock," *Proceedings of the National Academy of Sciences*, vol. 111, no. 21, pp. 7807–7812, 2014.

[138] B. Božič, Š. Zemljič Jokhadar, L. Kristanc, and G. Gomišček, "Cell volume changes and membrane ruptures induced by hypotonic electrolyte and sugar solutions," *Frontiers in Physiology*, vol. 11, p. 582 781, 2020.

Chapter 6

Supplementary Material

For the convenience of the reader, supplementary information and additional details regarding the main equations have been organized into this section.

Additional terms in Eq 4.1 in Mathematical Model section:

$$W = kH^2 + \bar{k}K + \frac{1}{2}E_1\varepsilon_1^2 + \frac{1}{2}E_2\varepsilon_2^2 + \frac{1}{2}C(\mathbf{g_1}\cdot\mathbf{g_1} + \frac{1}{2}\mathbf{g_2}\cdot\mathbf{g_2}) + \frac{1}{2}D\mathbf{g_1}\cdot\mathbf{g_2}$$

$$H = \frac{1}{2}a^{\alpha\beta}b_{\alpha\beta}$$

$$K = \frac{1}{2}\varepsilon^{\alpha\beta}\varepsilon^{\lambda\mu}b_{\alpha\lambda}b_{\beta\mu}$$

$$\varepsilon_1 = \frac{1}{2}(\lambda^2 - 1) = \frac{1}{2}(\mathbf{FL}\cdot\mathbf{FL} - 1) = \frac{1}{2}(\chi_{1,1}\chi_{1,1} + \chi_{2,1}\chi_{2,1} + \chi_{3,1}\chi_{3,1} - 1)$$

$$\varepsilon_2 = \frac{1}{2}(\mu^2 - 1) = \frac{1}{2}(\mathbf{FM} \cdot \mathbf{FM} - 1) = \frac{1}{2}(\chi_{1,2}\chi_{1,2} + \chi_{2,2}\chi_{2,2} + \chi_{3,2}\chi_{3,2} - 1)$$

$$\mathbf{g_1} = \bigtriangledown \mathbf{F}(\mathbf{L} \otimes \mathbf{L})$$

$$\mathbf{g_2} = \bigtriangledown \mathbf{F}(\mathbf{M} \otimes \mathbf{M})$$

$$(\frac{1}{2}\mathbf{g_1} \cdot \mathbf{g_1})^{\cdot} = u^{\alpha}[(\Gamma^{\varepsilon}_{jK})_{,Bi}a_{\varepsilon\alpha} + (\Gamma^{\varepsilon}_{jK})_{,B}\Gamma^{g}_{\varepsilon i}a_{g\alpha} + (\Gamma^{\varepsilon}_{jK}\Gamma^{m}_{\varepsilon B})_{,i}a_{m\alpha} + \Gamma^{\varepsilon}_{jK}\Gamma^{m}_{\varepsilon B}\Gamma^{h}_{mi}a_{h\alpha} - \Gamma^{\varepsilon}_{jK}b_{\varepsilon B}b^{p}_{i}a_{p\alpha} -$$

$$(\mathrm{b}_{jK})_{,B}b^{q}_{i}a_{q\alpha} - (b_{jK}b^{k}_{B})_{,i}a_{k\alpha} - b_{jK}b^{k}_{B}\Gamma^{w}_{ki}a_{w\alpha}]L_iL_BL_jL_K + u[(\Gamma^{\varepsilon}_{jK})_{,B}b_{\varepsilon i} + \Gamma^{\varepsilon}_{jK}\Gamma^{m}_{\varepsilon B}b_{mi} +$$

$$(\Gamma^{\varepsilon}_{jK}b_{\varepsilon B})_{,i} + (b_{jK})_{,iB} - b_{jK}b^{k}_{B}b_{ki}]L_iL_BL_jL_Kda + L_iL_BL_jL_K[(\mathbf{a}_{j,K} \cdot \mathbf{u}_{,i})_{,B} - (\mathbf{a}_{j,KB} \cdot \mathbf{u})_{,i}]$$

$$(\frac{1}{2}\mathbf{g_2} \cdot \mathbf{g_2})^{\cdot} = u^{\alpha}[(\Gamma^{\varepsilon}_{jK})_{,Bi}a_{\varepsilon\alpha} + (\Gamma^{\varepsilon}_{jK})_{,B}\Gamma^{g}_{\varepsilon i}a_{g\alpha} + (\Gamma^{\varepsilon}_{jK}\Gamma^{m}_{\varepsilon B})_{,i}a_{m\alpha} + \Gamma^{\varepsilon}_{jK}\Gamma^{m}_{\varepsilon B}\Gamma^{h}_{mi}a_{h\alpha} - \Gamma^{\varepsilon}_{jK}b_{\varepsilon B}b^{p}_{i}a_{p\alpha} -$$

$$(\mathrm{b}_{jK})_{,B}b^{q}_{i}a_{q\alpha} - (b_{jK}b^{k}_{B})_{,i}a_{k\alpha} - b_{jK}b^{k}_{B}\Gamma^{w}_{ki}a_{w\alpha}]M_iM_BM_jM_K + u[(\Gamma^{\varepsilon}_{jK})_{,B}b_{\varepsilon i} + \Gamma^{\varepsilon}_{jK}\Gamma^{m}_{\varepsilon B}b_{mi} +$$

$$(\Gamma^{\varepsilon}_{jK}b_{\varepsilon B})_{,i} + (b_{jK})_{,iB} - b_{jK}b^{k}_{B}b_{ki}]M_iM_BM_jM_K + M_iM_BM_jM_K[(\mathbf{a}_{j,K} \cdot \mathbf{u}_{,i})_{,B} - (\mathbf{a}_{j,KB} \cdot \mathbf{u})_{,i}]$$

$$(\frac{1}{2}\mathbf{g_1}\cdot\mathbf{g_2})^{\cdot} = \frac{1}{2}u^{\alpha}[(\Gamma^{\varepsilon}_{jK})_{,Bi}a_{\varepsilon\alpha}+(\Gamma^{\varepsilon}_{jK})_{,B}\Gamma^{g}_{\varepsilon i}a_{g\alpha}+(\Gamma^{\varepsilon}_{jK}\Gamma^{m}_{\varepsilon B})_{,i}a_{m\alpha}+\Gamma^{\varepsilon}_{jK}\Gamma^{m}_{\varepsilon B}\Gamma^{h}_{mi}a_{h\alpha}-\Gamma^{\varepsilon}_{jK}b_{\varepsilon B}b^{p}_{i}a_{p\alpha}-$$

$$(b_{jK})_{,B}b^{q}_{i}a_{q\alpha}-(b_{jK}b^{k}_{B})_{,i}a_{k\alpha}-b_{jK}b^{k}_{B}\Gamma^{w}_{ki}a_{w\alpha}]M_iM_BL^jL^K+$$

$$\frac{1}{2}u[(\Gamma^{\varepsilon}_{jK})_{,B}b_{\varepsilon i}+\Gamma^{\varepsilon}_{jK}\Gamma^{m}_{\varepsilon B}b_{mi}+(\Gamma^{\varepsilon}_{jK}b_{\varepsilon B})_{,i}+(b_{jK})_{,iB}-b_{jK}b^{k}_{B}b_{ki}]M_iM_BL^jL^K+$$

$$\frac{1}{2}u^{\alpha}[(\Gamma^{\varepsilon}_{jK})_{,Bi}a_{\varepsilon\alpha}+(\Gamma^{\varepsilon}_{jK})_{,B}\Gamma^{g}_{\varepsilon i}a_{g\alpha}+(\Gamma^{\varepsilon}_{jK}\Gamma^{m}_{\varepsilon B})_{,i}a_{m\alpha}+\Gamma^{\varepsilon}_{jK}\Gamma^{m}_{\varepsilon B}\Gamma^{h}_{mi}a_{h\alpha}-\Gamma^{\varepsilon}_{jK}b_{\varepsilon B}b^{p}_{i}a_{p\alpha}-$$

$$(b_{jK})_{,B}b^{q}_{i}a_{q\alpha}-(b_{jK}b^{k}_{B})_{,i}a_{k\alpha}-b_{jK}b^{k}_{B}\Gamma^{w}_{ki}a_{w\alpha}]M_jM_KL^iL^B+$$

$$\frac{1}{2}u[(\Gamma^{\varepsilon}_{jK})_{,B}b_{\varepsilon i}+\Gamma^{\varepsilon}_{jK}\Gamma^{m}_{\varepsilon B}b_{mi}+(\Gamma^{\varepsilon}_{jK}b_{\varepsilon B})_{,i}+(b_{jK})_{,iB}-b_{jK}b^{k}_{B}b_{ki}]M_jM_KL^iL^B+$$

$$\frac{1}{2}(M_iM_BL^jL^K+M_jM_KL^iL^B)[(\mathbf{a}_{j,K}\cdot\mathbf{u}_{,i})_{,B}-(\mathbf{a}_{j,KB}\cdot\mathbf{u})_{,i}].$$

Additional terms in Eq 4.10 in Mathematical Model section:

$$\Delta(\frac{1}{2}W_H)+(W_K)_{;\beta\alpha}\tilde{b}^{\beta\alpha}+W_H(2H^2-K)+2KHW_K-2H(W+\lambda)-$$

$$\frac{E_1}{2}(a_{mn}L_mL_n-1)L_iL_jb_{ji}-\frac{E_2}{2}(a_{mn}M_mM_n-1)M_iM_jb_{ji}+$$

$$C[(\Gamma^{\varepsilon}_{jK})_{,B}b_{\varepsilon i}+\Gamma^{\varepsilon}_{jK}\Gamma^{m}_{\varepsilon B}b_{mi}+(\Gamma^{\varepsilon}_{jK}b_{\varepsilon B})_{,i}+(b_{jK})_{,iB}-b_{jK}b^{k}_{B}b_{ki}]L_iL_BL_jL_K+$$

$$C[(\Gamma^{\varepsilon}_{jK})_{,B}b_{\varepsilon i}+\Gamma^{\varepsilon}_{jK}\Gamma^{m}_{\varepsilon B}b_{mi}+(\Gamma^{\varepsilon}_{jK}b_{\varepsilon B})_{,i}+(b_{jK})_{,iB}-b_{jK}b^{k}_{B}b_{ki}]M_iM_BM_jM_K+$$

$$\frac{D}{2}[(\Gamma^{\varepsilon}_{jK})_{,B}b_{\varepsilon i}+\Gamma^{\varepsilon}_{jK}\Gamma^{m}_{\varepsilon B}b_{mi}+(\Gamma^{\varepsilon}_{jK}b_{\varepsilon B})_{,i}+(b_{jK})_{,iB}-b_{jK}b^{k}_{B}b_{ki}]M_iM_BL^jL^K+$$

$$\frac{D}{2}[(\Gamma^{\varepsilon}_{jK})_{,B}b_{\varepsilon i}+\Gamma^{\varepsilon}_{jK}\Gamma^{m}_{\varepsilon B}b_{mi}+(\Gamma^{\varepsilon}_{jK}b_{\varepsilon B})_{,i}+(b_{jK})_{,iB}-b_{jK}b^{k}_{B}b_{ki}]M_jM_KL^iL^B=P$$